NAVAL POSTGRADUATE SCHOOL

MONTEREY, CALIFORNIA

THESIS

DIGITAL ANTENNA ARCHITECTURES USING COMMERCIAL OFF THE SHELF HARDWARE

by

Eng, Cher Shin

December 2003

Thesis Advisor:	David C. Jenn
Second Reader:	Roberto Cristi

Approved for public release; distribution is unlimited.

THIS PAGE INTENTIONALLY LEFT BLANK

REPORT DOCUMENTATION PAGE			Form Approved OMB No. 0704-0188
Public reporting burden for this collection of information is estimated to average 1 hour per response, including the time for reviewing instruction, searching existing data sources, gathering and maintaining the data needed, and completing and reviewing the collection of information. Send comments regarding this burden estimate or any other aspect of this collection of information, including suggestions for reducing this burden, to Washington headquarters Services, Directorate for Information Operations and Reports, 1215 Jefferson Davis Highway, Suite 1204, Arlington, VA 22202-4302, and to the Office of Management and Budget, Paperwork Reduction Project (0704-0188) Washington DC 20503.			
1. AGENCY USE ONLY *(Leave blank)*	**2. REPORT DATE** December 2003	**3. REPORT TYPE AND DATES COVERED** Master's Thesis	
4. TITLE AND SUBTITLE: Digital Antenna Architectures Using Commercial Off The Shelf Hardware			**5. FUNDING NUMBERS**
6. AUTHOR(S) ENG, Cher Shin			
7. PERFORMING ORGANIZATION NAME(S) AND ADDRESS(ES) Naval Postgraduate School Monterey, CA 93943-5000			**8. PERFORMING ORGANIZATION REPORT NUMBER**
9. SPONSORING /MONITORING AGENCY NAME(S) AND ADDRESS(ES) N/A			**10. SPONSORING/MONITORING AGENCY REPORT NUMBER**
11. SUPPLEMENTARY NOTES The views expressed in this thesis are those of the author and do not reflect the official policy or position of the Department of Defense or the U.S. Government.			
12a. DISTRIBUTION / AVAILABILITY STATEMENT Approved for public release; distribution is unlimited.			**12b. DISTRIBUTION CODE**

13. ABSTRACT (maximum 200 words)

The changes in war fighting tactics and advancement of technology shape the ways to implement and design multifunction phased array radars. This thesis investigated whether the commercial modulation boards used in the 3-D 2.4-GHz phased array transmit antenna is capable of wideband performance. The phase of the transmitted signal out of the modulator board was adjusted to provide a phase shift from 0 to 2π, and the insertion phases at these phase settings were measured using a Vector Network Analyzer, sweeping the frequency from 0.8 to 2.5 GHz. The measured insertion phases are used to simulate the radiation pattern of a linear phased array, and the results show that modulator does not have instantaneous wideband characteristics.

This thesis also looked at the design of the complementary phased array receiver architecture using commercially available demodulator boards. The demodulator board was successfully configured to operate as a phase shifter. Phase shifted transmit signals were injected into the demodulator, and corresponding phase shifts were measured via the *In-Phase* and *Quadrature* voltages.

14. SUBJECT TERMS Phased Array, Array Bandwidth, Beamforming, Radar, Antenna, Transmitter, Receiver, Direction Finding, Modulation, Demodulation, COTS.			**15. NUMBER OF PAGES** 96
			16. PRICE CODE
17. SECURITY CLASSIFICATION OF REPORT Unclassified	**18. SECURITY CLASSIFICATION OF THIS PAGE** Unclassified	**19. SECURITY CLASSIFICATION OF ABSTRACT** Unclassified	**20. LIMITATION OF ABSTRACT** UL

NSN 7540-01-280-5500 Standard Form 298 (Rev. 2-89)
Prescribed by ANSI Std. 239-18

THIS PAGE INTENTIONALLY LEFT BLANK

Approved for public release; distribution is unlimited.

DIGITAL ANTENNA ARCHITECTURES
USING COMMERCIAL OFF-THE-SHELF HARDWARE

Cher Shin Eng
Civilian, Ministry of Defense, Singapore
B.E., Queensland University of Technology, Australia, 1998

Submitted in partial fulfillment of the
requirements for the degree of

MASTER OF SCIENCE IN ENGINEERING SCIENCE
(ELECTRICAL ENGINEERING)

from the

NAVAL POSTGRADUATE SCHOOL
December 2003

Author: Cher Shin Eng

Approved by: David C. Jenn
Thesis Advisor

Roberto Cristi
Second Reader

John P. Powers
Chairman, Department of Electrical and Computer Engineering

THIS PAGE INTENTIONALLY LEFT BLANK

ABSTRACT

The changes in war fighting tactics and advancement of technology shape the ways to implement and design multifunction phased array radars. This thesis investigated whether the commercial modulation boards used in the 3-D 2.4-GHz phased array transmit antenna is capable of wideband performance. The phase of the transmitted signal out of the modulator board was adjusted to provide a phase shift from 0 to 2π, and the insertion phases at these phase settings were measured using a Vector Network Analyzer, sweeping the frequency from 0.8 to 2.5 GHz. The measured insertion phases are used to simulate the radiation pattern of a linear phased array, and the results show that the modulator does not have instantaneous wideband characteristics.

This thesis also looked at the design of the complementary phased array receiver architecture using commercially available demodulator boards. The demodulator board was successfully configured to operate as a phase shifter. Phase shifted transmit signals were injected into the demodulator, and corresponding phase shifts were measured via the *In-Phase* and *Quadrature* voltages.

THIS PAGE INTENTIONALLY LEFT BLANK

TABLE OF CONTENTS

LIST OF FIGURES

LIST OF TABLES

THIS PAGE INTENTIONALLY LEFT BLANK

ACKNOWLEDGMENTS

I would like to express our most sincere gratitude to Professor David Jenn of the Naval Postgraduate School, Monterey, California for his guidance and invaluable contributions to the completion of this work. He has never failed to stop whatever work he is doing to attend to my questions and I really appreciate it.

I would also like to thank Professor Roberto Cristi for agreeing to be my second reader to this thesis and also acting a mentor to the group of students from the Temasek Defense Systems Institute (TDSI), providing supports and guidance.

THIS PAGE INTENTIONALLY LEFT BLANK

EXECUTIVE SUMMARY

Operation in a littoral environment calls for a ship self-defense system capable of coping with a high intensity, combined missile, aircraft and surface threats, under severe jamming and clutter conditions. One of the important components of the ship self-defense philosophy is stealth technology, or signature control.

In addition, operation in a littoral environment demands that the radar system provide long range detection and accurate tracking, and this implies physically large radar antennas with high gain and narrow beamwidth. However, this requirement conflicts with the stealth technology requirement, putting constraints on the design of the warship.

A possible solution to the conflicting requirements is to design a warship's structure to possess all the necessary stealth characteristics, and then integrate into the ship's structure several smaller noncontiguous subarray antennas that process the received signal coherently. These subarray elements not only serve as an aperture for radar applications, but also serve as apertures for a wide spectrum communication applications.

Unlike the military hardware of the past, information technology is advancing at a pace driven not by the military's requirements, but by the industrial and consumer sectors. These phenomena are mostly due to the development of Commercial-off-the-Shelf (COTS) microchips. Number-crunching chips are becoming more powerful while their cost and physical size are shrinking. Thus engineers should exploit commercial technologies for radar and communications applications.

Digital antennas have the potential to satisfy these diverse requirements simultaneously. The ideal digital antenna has the following features:

1. Potential ultra-wideband performance,
2. Use of distributed noncontiguous areas of the ship or aircraft for the antenna aperture,

3. Ability to serve several systems and perform multiple functions simultaneously (e.g., multiple beams, direction finding, search and track, and communications),
4. Low cost through the implementation of COTS,
5. Flexibility to change system parameters with simple software modifications.

This thesis is the continuation of research on a 3-D 2.4-GHz digital phased array radar antenna carried out at the Naval Postgraduate School. This thesis investigated whether the commercial modulator board used in the phased array transmit antenna is capable of wideband performance. The phase of the transmitted signal out of the modulator board was adjusted to provide a phase shift from 0 to 2π, and the insertion phases at these phase settings were measured using a Vector Network Analyzer, sweeping the frequency from 0.8 to 2.5 GHz. The effects of the phase slope and amplitude variations on the pattern of a linear array were determined by simulations that incorporated the measured data. The simulation showed that the instantaneous bandwidth of the modulator board is much narrower than the specified frequency range of operation (0.8 to 2.5 GHz). Thus, this modulator board does not have wide instantaneous bandwidth characteristics.

This thesis also looked at the design of the complementary phased array receiver architecture using commercial Radio Frequency (RF) microchips. The operating characteristics of an available quadrature demodulator were studied, and the results are presented. The demodulator was successfully configured to operate as a phase shifter. Phase shifted transmit signals from the modulator board were injected into the demodulator, and corresponding phase shifts were measured via the *In-phase* and *Quadrature* voltages. A periodic phase error was identified and attributed to the phase error inherent in the modulator board.

I. INTRODUCTION

A. MOTIVATION

Radar continues to be the principal above-water sensor for surface combatants. However, changes in the global security situation have led to navies sending their warships to operate much closer to potentially hostile coasts, e.g., in the Persian Gulf, as opposed to traditional operations in the open ocean. The operation in a littoral environment calls for a ship self-defense system capable of coping with a high intensity, combined missile, aircraft and surface threats, under severe jamming and clutter conditions.

One of the important components of the ship self defense philosophy is stealth technology, or signature control. Warships are now being designed for minimal platform signatures in the Radar Cross Section (RCS), Infrared (IR), magnetic, and acoustic domains. The design of minimal RCS and IR signatures, on one hand, calls for a small-integrated superstructure of the warship, which implies reduced area for sensors and weapon systems. On the other hand, the threats in the littoral environment require the radar to provide long-range detection and accurate tracking, and this implies physically large radar antennas with high gain and narrow beamwidth. Current radar array antennas are large planar arrays and easily recognizable, e.g., the SPY-1 radar used in the AEGIS combat systems, shown in Figure 1. These array antennas and their support structures are a primary driving factor in the design and construction of a warship.

Figure 1. SPY-1 Antenna Face (From Ref. [1].).

A possible solution to the conflicting design requirements is to define the warship's structure that possesses all of the necessary stealth characteristics, as well as maximized survivability and maneuverability, and then to integrate into the ship's structure several smaller noncontiguous subarray antennas that process the received signal coherently. A radar designed in this way would have good angular resolution since the angular resolution (i.e., half power beamwidth, θ_B) is proportional to the ratio of wavelength over the aperture width of the array as given by

$$\theta_B = 65\frac{\lambda}{D}, \tag{1}$$

where λ is the wavelength and D is the dimension of the antenna. Thus, the aperture width could potentially be the overall length of the warship. These integrated ship-wide subarray antennas are evident in the proposed new DD(X) class destroyer design, as illustrated in Figure 2. These array elements not only serve as an aperture for radar applications, but also serve as apertures for a wide spectrum of communication applications. A single antenna with wideband performance can eliminate the numerous antennas and masts populating the current ship superstructure. In addition, operating in the UHF/VHF frequency band has the advantages of longer range detection and anti-stealth.

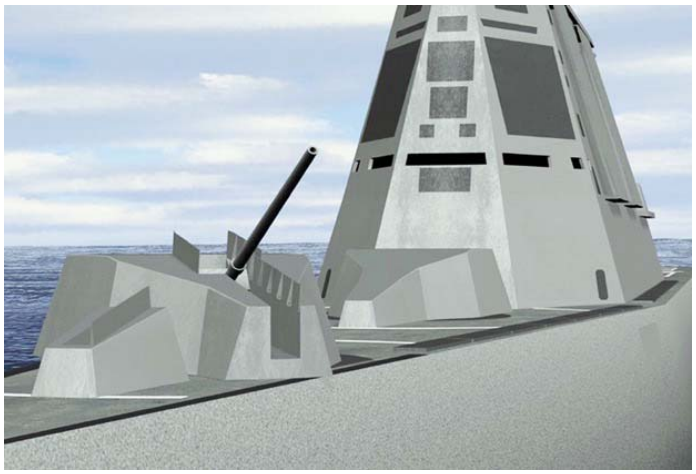

Figure 2. Subarray Antennas in the DD(X) Superstructure (From Ref. [2].).

Such a distributed subarray is possible through the use of a branch of computer programs known as Genetic Algorithms (GAs). The GA can determine the evolved array configuration that is compatible with the naval architecture's design criteria, instead of restricting the ship design due to radar location [3]. A more detailed description of the GA can be found in [3].

Today's naval radars have double the performance of those of the early nineteen eighty's, yet they cost the same [4]. In addition, unlike the military hardware of the past, information technology is advancing at a pace driven not by the military's requirements, but by the industrial and consumer sectors. These phenomena are mostly due to the development of Commercial-off-the-Shelf (COTS) microchips. Number-crunching chips are becoming more powerful while their cost and physical size are shrinking. Hence engineers have to leverage and evaluate commercial technologies for radar and communications architectures now and in the future.

Digital antennas have the potential to satisfy these diverse requirements simultaneously. The ideal digital antenna has the following features:

1. Potential ultra-wideband performance,
2. Use of distributed noncontiguous areas of the ship or aircraft for antenna aperture,

3. Ability to serve several systems and perform multiple functions simultaneously (e.g., multiple beams, direction finding, search and track, and communications),

4. Low cost through the implementation of COTS,

5. Flexibility to change system parameters with simple software modifications.

B. PREVIOUS WORK

This thesis is the continuation of the efforts to achieve a 3-D 2.4-GHz digital phased array radar. The transmit antenna design was carried out at the Naval Postgraduate School by LCDR Lance C. Esswein, USN [3]. Esswein had designed a phased array transmit antenna using COTS products and demonstrated that the GA program and its pattern builder function would form a radiation beam in agreement with the theoretical calculations.

The Analog Devices (AD) AD8346EVAL modulator boards were assembled into a twenty-four element array. These modulators boards were configured as phase shifters, each feeding one of twenty-four printed circuit dipoles acting as the radiating elements. Esswein verified that the radiation pattern measurements taken in the anechoic chamber were in good agreement with those predicted by numerical simulation.

C. SCOPE AND ORGANIZATION

1. Scope

In [3], only phase scanning at a single frequency of 2.4 GHz was used in the demonstration. As a continuation of the research, this thesis investigated whether the modulator board used in the phased array transmit antenna is capable of wideband performance. The phase of the transmitted signal out of the modulator board was adjusted to provide a phase shift from 0 to 2π, and the insertion phases at these phase settings were measured using a Vector Network Analyzer, sweeping the frequency from 0.8 to 2.5 GHz. The measured insertion phases were used to simulate the radiation pattern of a linear phased array.

This thesis also looked at the design of the complementary phased array receiver architecture using commercial Radio Frequency (RF) microchips. The operating characteristics of an available quadrature demodulator were studied, and the results are presented.

2. Primary Research Questions

There are two related research questions addressed in this thesis. The first was to examine the operating characteristics of the COTS modulator and demodulator for digital phased array applications. The second was to access possible digital antenna architectures that might use the COTS products.

3. Organization

Chapter II presents a brief overview of the phased array design addressing the calculation of the Array Factor (AF), wideband array characteristics and adaptive beamforming. The processes of direction finding and receiver demodulation are also discussed.

Chapter III provides the analysis of the measured scattering parameters (S_{21}) for the phased array transmit antenna in terms of amplitude and phase. In addition, these measured data are used to verify whether the modulator board has wideband performance by simulating radiation patterns of a linear phased array. The demodulator board for the phased array receiver is characterized and the results are presented.

Chapter IV contains the summary of the experimental results followed by suggestions for future research into the phased array architecture using COTS.

Appendix A is the glossary of terms and abbreviations used within this thesis. Appendix B is the MATLAB code for generating Figures 17 to 20. Appendix C is the MathCAD codes for simulating the radiation pattern of the linear phased array. Appendix D is the MATLAB code for the phased array receiver.

THIS PAGE INTENTIONALLY LEFT BLANK

II. PHASED ARRAYS

This chapter discusses the fundamental concept and theory of phased arrays such as array factor, bandwidth, and adaptive beamforming. The processes of direction finding and receiver demodulation are also discussed.

A. ARRAYS

A single element has relatively wide radiation pattern and it has low values of directivity and gain [5]. In many applications, especially radar defense systems, the antenna must have very directive characteristics and high gain to meet the demand of high resolution in both angle and range. This can be realized by two methods. The first method is to increase the electrical size of the antenna. The second is to form an assembly of radiating elements in an electrical and geometrical configuration without increasing the dimension of the individual elements. This second approach, formed by multi-elements, is referred to as an *array*.

Arrays offer the unique capability to steer the radar beam virtually instantaneously, without mechanical movement, in any required direction by simply changing the phase of the exciting currents in each element of the array. Such an array is called a *phased array*.

B. ARRAY FACTOR (AF)

A phased array can be geometrically constructed around a circle (circular array), along a line (linear array), on plane (planar array), or throughout a volume, as shown in Figure 3.

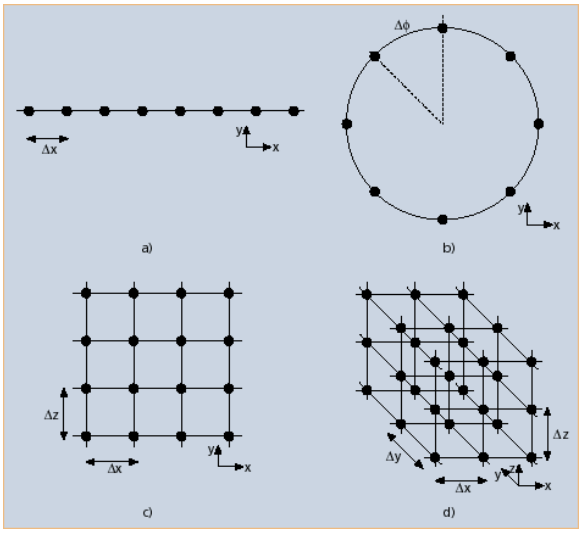

Figure 3. Different Array Geometries for Phased Array Antennas (From Ref. [6].).

For simplicity, the linear array is used to illustrate the concept of array factor. The array of Figure 4 has uniformly spaced identical isotropic radiators, positioned along the *x*-axis. The pattern characteristic of the array can be explained in either the transmit or receive mode, since the antenna usually satisfies the conditions for reciprocity [7].

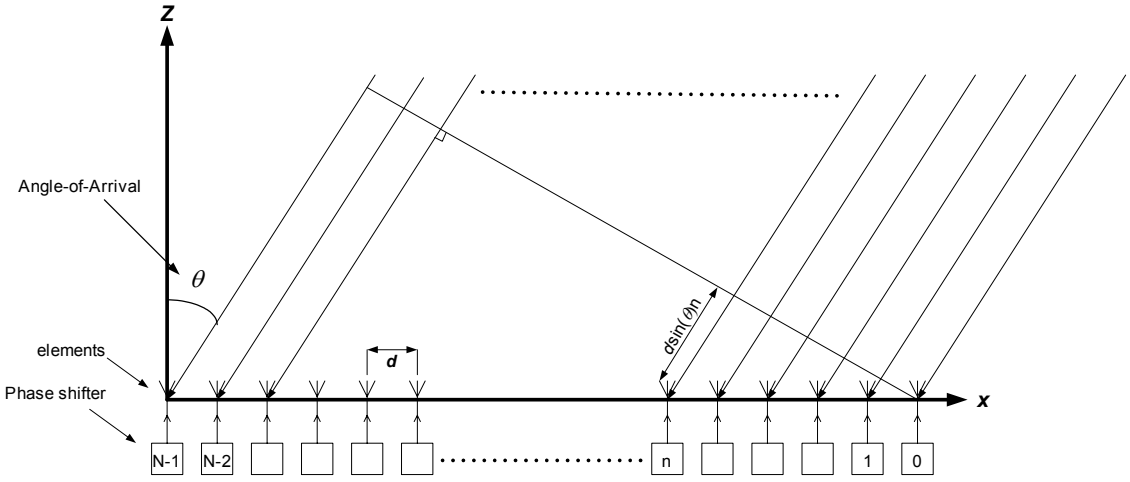

Figure 4. Geometry of the Uniformly Spaced Linear Array.

The parameter *d* represents the separation between antenna elements. Because the wave is incident at an angle θ relative to the axis of the array, all of the elements will receive the signal at different time, and thus be different in phase angle (i.e., phase shifted). We can determine the signal angle-of-arrival by measuring the phase difference

between the elements and then sum up all of the signals received by individual elements in order to maximize the received signal. Therefore by controlling the delays (phase shifts), we can select the direction of maximum reception or transmission for the array.

The array factor, AF for an N element uniform linear array along the x-axis is given by [5]

$$AF(\theta) = \sum_{n=0}^{N-1} A_n e^{j\Phi_n} e^{-j\frac{2\pi}{\lambda} nd\sin(\theta)}, \tag{2}$$

where

N = number of elements,

$A_n e^{j\Phi_n}$ = complex coefficient of element n used to steer the beam in the desired direction,

$= A_n e^{j\frac{2\pi}{\lambda} nd\sin(\theta_s)}$,

θ_s = scanning direction of the main beam,

d = spacing between elements in terms of wavelength,

λ = wavelength, and

A_n = magnitude of voltage or current at element n (assume all $A_n = 1$).

The far-field pattern of Equation (2) assumes that all the elements are identical and uniformly spaced. Isotropic elements have been assumed. If the elements are not isotropic, then the total radiation pattern of the array is the product of the element pattern and the array factor.

C. ARRAY BANDWIDTH

Equation (2) is valid for a single wavelength λ, i.e., narrowband, but in the wideband case, λ will cover a range of wavelengths. Hence Equation (2) is modified to accommodate the array pattern as a function of radiating frequency and angle. Substitute $\lambda = c/f$ in Equation (2) to obtain

$$AF(f,\theta) = \sum_{n=0}^{N\text{-}1} A_n(f) e^{j\frac{2\pi f}{c} nd \sin(\theta_s)} e^{-j\frac{2\pi f}{c} nd \sin(\theta)}, \quad (3)$$

where

$\Phi_n(f) = \frac{2\pi f}{c} nd \sin(\theta_s)$,
$A_n(f) =$ a set of real weights, and
$c =$ speed of light.

If the frequency (or wavelength) of operation changes, then a new set of phase shift settings is required to keep the beam location fixed. That is, the first exponent $\Phi_n(f)$ in Equation (3) must change with frequency in the same way that the second exponent changes with frequency. This would be a true time delay (TTD) phase shift. It will be shown that the COTS boards do not provide TTD. The phase shifter setting for a board is fixed for all frequencies. When the operating frequency changes, then the main beam will steer off from the desired direction, changing both in width and direction with frequency [8]. This effect is sometimes referred to as beam squint.

The beam squint is greater for a larger array aperture than a smaller array aperture in applications where a large array aperture and a large beamwidth are required for high range and angle resolutions. Reference [9] has suggested the solution to the beam squint problem is to introduce time delay units (TDU) at the sub-array level, so as to match the delays caused by the signal arriving at the different elements at different times.

A TDU is inserted into the feed path of each element. The signals that pass through the TDU are delayed by time ΔT. By properly selecting the delay value feeding each element, the transmitted (or received) wave front is fixed in the desired direction at all frequencies [10]. However, an analog TDU is undesirable because it becomes large for significant time delays at low frequencies. It may be possible to add the necessary time delay in the signal processing step of a digital antenna.

D. ADAPTIVE BEAMFORMING

As discussed in the above sections, a phased array can not only beam steer to the desired direction for transmission (or reception) but also simultaneously suppress the radiation pattern in the directions of the interferers as shown in the Figure 5. This process is known as adaptive beamforming and nulling.

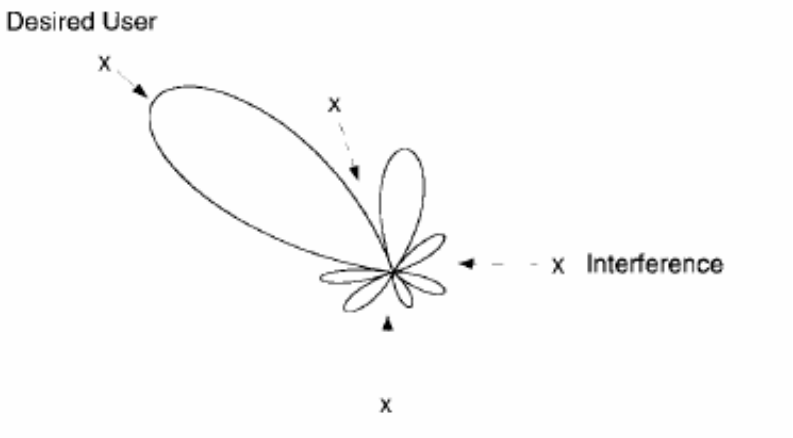

Figure 5. A Sample Array Pattern (From Ref. [11].).

Figure 5 shows that the mainbeam is steered to the desired user (or target) while at the same time, having nulls in the directions of the interferers. By doing so, the interference is minimized and the carrier-to-interference ratio for the desired user is maximized [11].

Reference [12] states that the maximum directivity of the linear array is proportional to the total length of the array (i.e., the length of the array can be increased by increasing the distance, usually described in terms of wavelength, between elements of the array). However there are some considerations for selecting the spacing between the antenna elements. If the antenna elements are spaced more than $\lambda/2$, grating lobes can appear, which cause undesirable effect on the radiation pattern of the array [12]. On the other hand, if the antenna elements are spaced less than $\lambda/4$, mutual coupling effects can occur that affect the radiation patterns and the impedance match. Thus the array performance will be degraded [12]. As a result, the separation dimensions between antenna elements typically ranges from $\lambda/4$ to $\lambda/2$.

E. DIRECTION FINDING

The basic principle of direction finding by an array antenna is described in the following paragraph using a two-element linear array model. The basic principle of a two-element linear array can then be extended to a larger number of elements. The details can be found in [13].

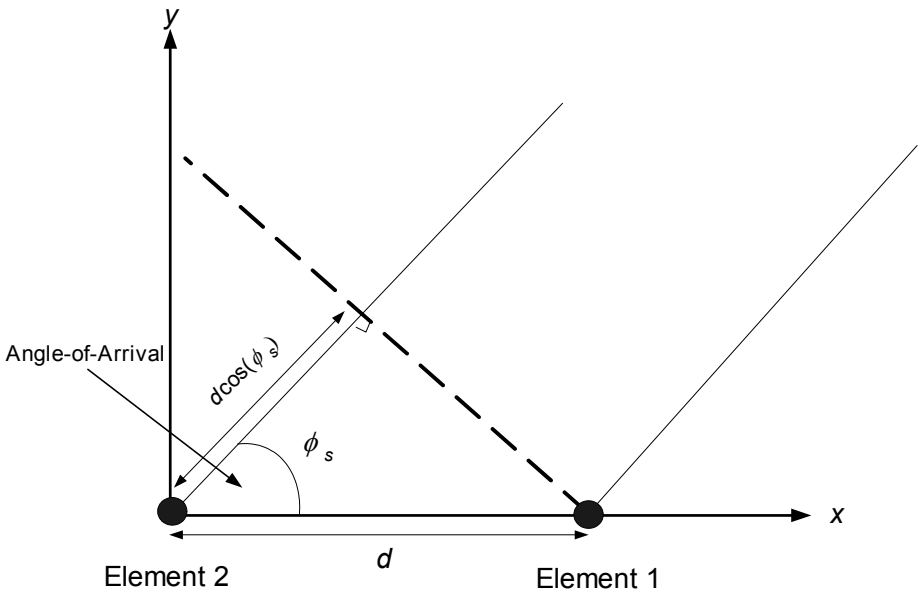

Figure 6. Two-Element Linear Array.

Figure 6 shows a two-element linear array positioned along the *x*-axis. Element two (2) receives the signal later than element one (1) as the wavefronts propagate toward the antenna with a propagation delay value $\tau_d = d\cos(\phi_s)/c$. Assume that the incoming narrowband signal has the following expression:

$$\begin{aligned} x(t) &= A(t)\cos\left(\omega_c t + \psi(t)\right) \\ &= A(t)\cos\psi(t)\cos(\omega_c t) - A(t)\sin\psi(t)\sin(\omega_c t) \\ &= x_1(t), \end{aligned} \tag{4}$$

where

$A(t) =$ amplitude of incoming signal,
$\psi(t) =$ phase of incoming signal,
$\omega_c = 2\pi f_c$, and
$x_1(t) =$ signal received by element one.

Similarly the incoming signal received by element two has the following expression:

$$\begin{aligned} x_2(t) &= A(t+\tau_d)\cos\left(\omega_c(t+\tau_d)+\psi(t+\tau_d)\right) \\ &= A(t+\tau_d)\cos[\psi(t+\tau_d)+\omega_c\tau_d]\cos(\omega_c t) \\ &\quad - A(t+\tau_d)\sin[\psi(t+\tau_d)+\omega_c\tau_d]\sin(\omega_c t). \end{aligned} \tag{5}$$

The delay τ_d can be assumed a function of the carrier period, because the incoming signal is assumed to be narrowband. Thus Equation (5) is modified to the following expression:

$$x_2(t) = A(t)\cos[\psi(t)+\omega_c\tau_d]\cos(\omega_c t) - A(t)\sin[\psi(t)+\omega_c\tau_d]\sin(\omega_c t), \tag{6}$$

where

$A(t) \simeq A(t+\tau_d)$ and
$\psi(t) \simeq \psi(t+\tau_d)$.

The incoming signals are received by the receiver circuit for each of the elements as shown in Figure 7.

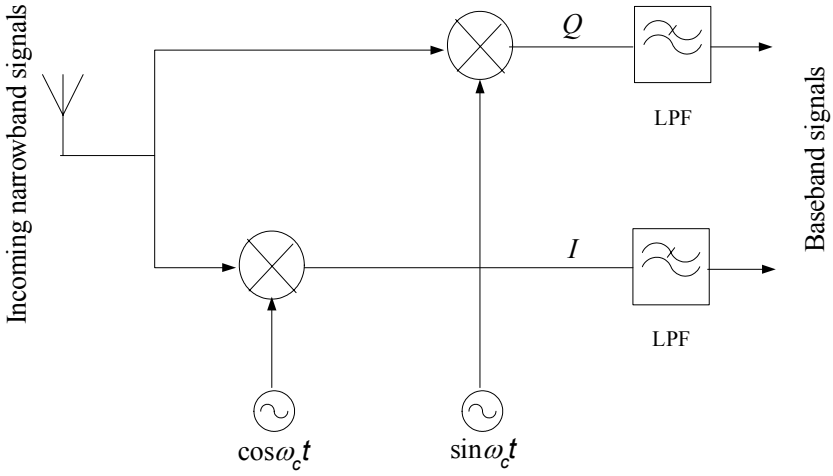

Figure 7. Receiver Circuit for an Element of the Array.

The narrowband incoming signals are demodulated to their respective baseband signals by the receiver circuit as shown in the following expressions for each of the elements. The *I* and *Q* are referred to as the in-phase and quadrature terms, respectively.

For element one, we can write:

$$\begin{aligned} I_1(t) &= A(t)\cos\left(\psi(t)\right) \\ Q_1(t) &= A(t)\sin\left(\psi(t)\right) \end{aligned} \tag{7}$$

while for element two:

$$\begin{aligned} I_2(t) &= A(t)\cos\left(\psi(t)\right)\cos\left(kd\cos\left(\phi_s\right)\right) - A(t)\sin\left(\psi(t)\right)\sin\left(kd\cos\left(\phi_s\right)\right) \\ Q_2(t) &= A(t)\cos\left(\psi(t)\right)\sin\left(kd\cos\left(\phi_s\right)\right) - A(t)\sin\left(\psi(t)\right)\cos\left(kd\cos\left(\phi_s\right)\right) \end{aligned} \tag{8}$$

where $kd\cos\left(\phi_s\right) = \omega_c \tau_c$.

The phase of the Local Oscillator (LO) in the receiver is adjusted such that $I_1(t)$ is maximized and $Q_1(t)$ is zero. The receiver is synchronized at the reference element with the incoming signal. Thus, in such a case $\psi(t) = 0$, which simplifies the expressions to

$$
\begin{aligned}
I_1(t) &= A(t) \\
Q_1(t) &= 0 \\
I_2(t) &= A(t)\cos\left(kd\cos\left(\phi_s\right)\right) \\
Q_2(t) &= A(t)\sin\left(kd\cos\left(\phi_s\right)\right).
\end{aligned}
\tag{9}
$$

As a result, the ratio of the two in-phase signals can be used to determine the angle of arrival

$$
\begin{aligned}
\frac{I_2(t)}{I_1(t)} &= \frac{A(t)\cos(kd\cos(\phi_s))}{A(t)} \\
&= \cos\left[kd\cos(\phi_s)\right]
\end{aligned}
\tag{10}
$$

which gives

$$
\phi_s = \cos^{-1}\left(\frac{1}{kd}\cos^{-1}\left(\frac{I_2(t)}{I_1(t)}\right)\right). \tag{11}
$$

Equation (11) assumes that the carrier frequency is known a-priori and is noise free. Also, that the $I_{1,2}(t)$ and $Q_{1,2}(t)$ values can be measured from the receiver. The drawback of a linear array is that the ϕ_s has the front-back ambiguity (i.e., two possible solutions).

F. *I* AND *Q* AND DEMODULATION SCHEME

Equation (7) can be used to demonstrate the *I* and *Q* demodulation scheme. In-phase and quadrature detection is able to recover a baseband signal without losing any information, by using Equation (7) [14]. The amplitude and phase can be recovered by

$$
A = \sqrt{I^2 + Q^2} \tag{12}
$$

and

$$
\psi = \tan^{-1}\left(\frac{Q}{I}\right). \tag{13}
$$

G. DIGITAL ANTENNA ARCHITECTURE

The basic architecture of a digital phased array transmit antenna is shown in Figure 8.

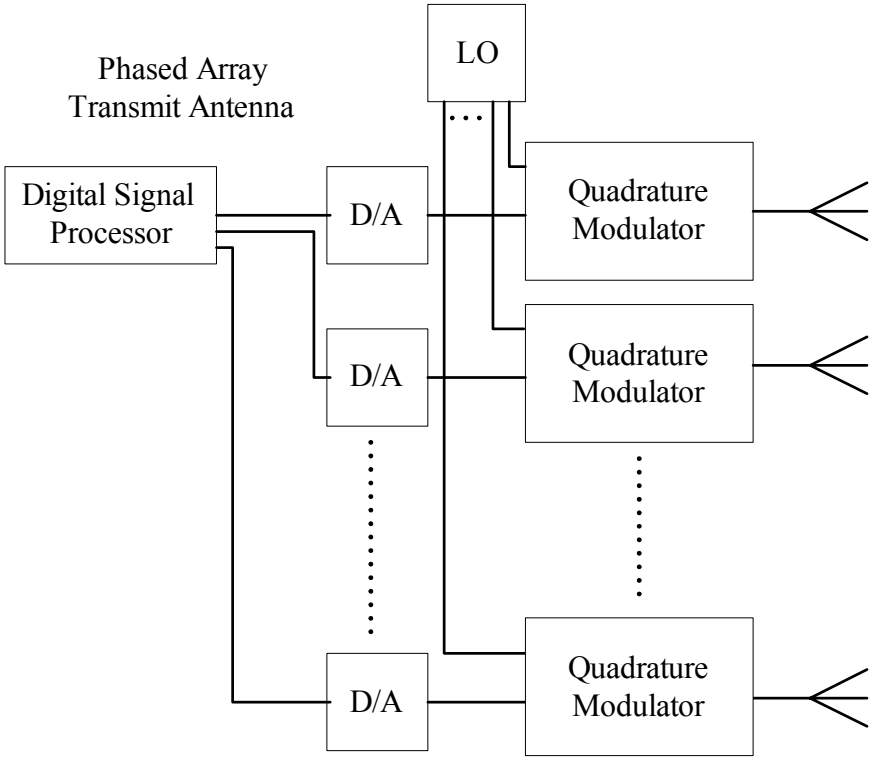

Figure 8. Architecture of a Digital Phased Array Transmit Antenna.

The transmit antenna is comprised of (1) a Digital Signal Processor (DSP), (2) multiple Digital-to-Analog Converters (DACs), (3) multiple modulator boards, (4) a Local Oscillator (LO) generator, and (5) multiple antenna elements.

The DSP is the brain of the digital antenna; it has the algorithms to compute the necessary complex coefficients required for beamforming. The data from the DSP is then converted from digital format to analog format before sending to the multiple modulators. The modulator, which performs as a phase shifter and amplitude controller in the digital antenna, modulates the analog data from the DAC with a carrier signal. The carrier signals for the multiple modulators are phase coherent and supplied by a LO generator. The phased shifted signals are then fed to the multiple antenna elements for transmission.

The digital phased array receive antenna performs the reverse function of the transmit antenna, and the basic architecture is shown Figure 9. The LO generator supplies the LO carrier signal to the demodulators in order for the demodulators to down convert the received signals to baseband signals. The baseband signals are then converted from analog format to digital format by the Analog-to-Digital Converters (ADCs) before sending them to the DSP for processing.

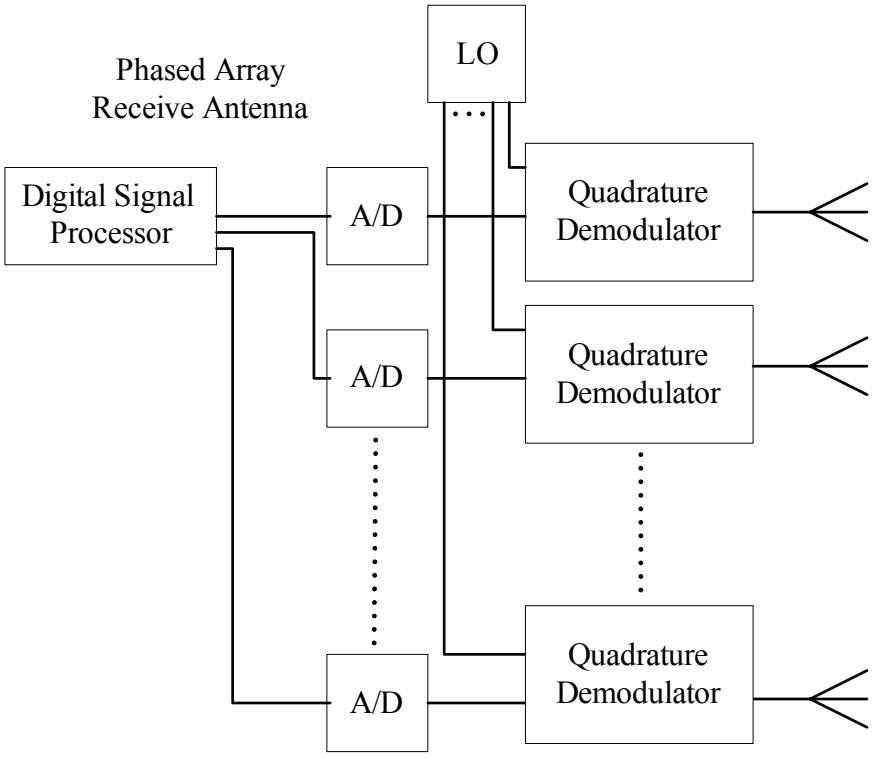

Figure 9. Architecture of a Digital Phased Array Receive Antenna.

H. SUMMARY

This chapter has presented the basic concept of arrays and also discussed some of the capabilities that the arrays have. This research focuses on the application of commercial modulators and demodulators to perform as phase shifters as described Section G. In addition, Equation (2) will be used in Chapter III, Section 4 to generate the radiation patterns of a linear array using MathCAD.

In the next chapter, both the commercial modulator and demodulator boards are experimentally configured, and their measured amplitudes and phases are obtained for analysis.

THIS PAGE INTENTIONALLY LEFT BLANK

III. DESIGN SELECTION AND MEASUREMENT ANALYSIS

This chapter provides the analysis of the measured scattering parameters (S_{21}) for the phased array transmit antenna in terms of amplitude and phase. In addition, these measured data are used to verify whether the modulator board has wideband performance by simulating radiation patterns of a linear phased array. The demodulator board for the phased array receiver is characterized and the results are presented.

A. THREE-DIMENSIONAL 2.4-GHZ PHASED ARRAY TRANSMIT ANTENNA

A 3-D 2.4-GHz phased array transmit antenna was designed and built by Lance C. Esswein [3]. The intent of his research was to assess whether the GA could be used as a design and beamforming tool for transmitting phased arrays, and whether commercially available RF microchips could be used to build the transmitting phased array antenna. The measurement results obtained from the constructed phased array antenna fully met the stated objectives. The details of his thesis can be found in [3].

In this thesis, the bandwidth characteristics (i.e., phase versus frequency response, and amplitude versus frequency response) of the Analog Devices AD8346EVAL Quadrature Modulator board are investigated.

1. AD8346EVAL Quadrature Modulator

The AD8346EVAL board is a silicon RF Integrated Circuit (RFIC) I/Q modulator that is normally used as the transmit modulator in digital systems such as Code Division Multiple Access (CDMA) and Global Satellite Mobile (GSM) transceivers. However, in [3], this modulator board was configured as a phase shifter for use in a digital 3-D phased array antenna.

The AD8346EVAL board has an operating frequency range from 0.8 GHz to 2.5 GHz [15] and, as such, this feature makes the modulator a potential component in wideband antennas for many sensor and communication applications.

2. Operation of the AD8346EVAL Board as a Phase Shifter

The following paragraph describes the controlling information necessary to operate the AD8346EVAL board as a phase shifter.

There are four input pins used for phase control namely (1) in-phase negative (IN), (2) in-phase positive (IP), (3) quadrature negative (QN), and (4) quadrature positive (QP). The phase shift quadrant determines which two pins receive positive control voltage signals while the other two pins are set to zero according to [3]. Figure 10 indicates the control pin combinations used in each of the quadrants while Table 1 shows the amount of control voltage needed for each pin in order to set the appropriate phase.

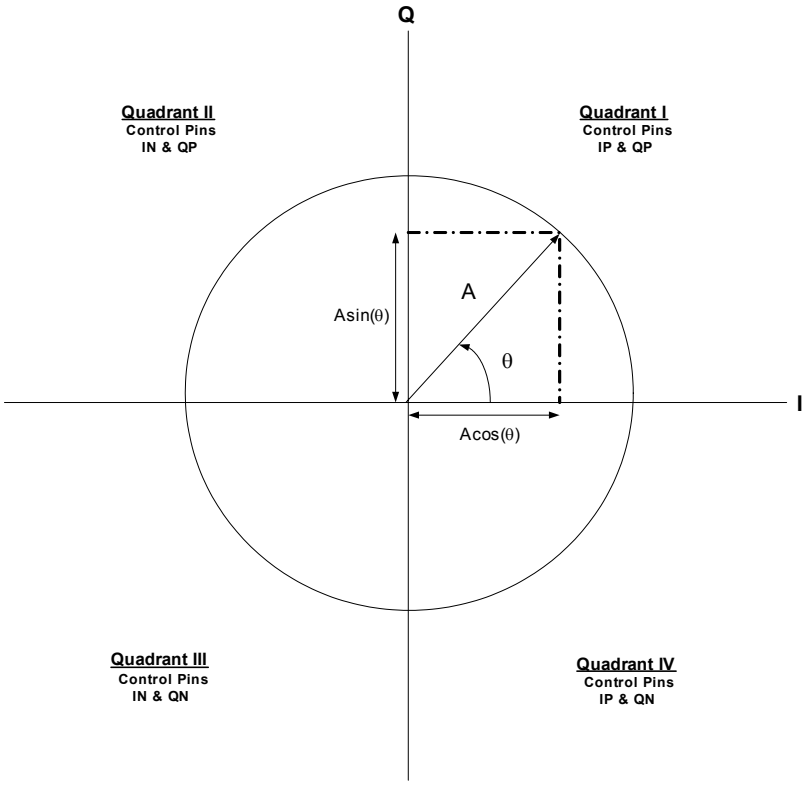

Figure 10. Complex (Phasor) Plane (From Ref. [3].).

Signal / Phase Shift	IN	IP	QP	QN
000-090	0	cos(θ)	sin(θ)	0
090-180	cos(θ)	0	sin(θ)	0
180-270	cos(θ)	0	0	sin(θ)
270-360	0	cos(θ)	0	sin(θ)

Table 1. Control Signal Value for Phase Shift (From Ref. [3].).

3. Magnitude and Phase Measurements for the AD8346EVAL Board

The AD8346EVAL board is configured as shown in Figure 11 to take the magnitude and phase measurements using a HP8510 Vector Network Analyzer (VNA).

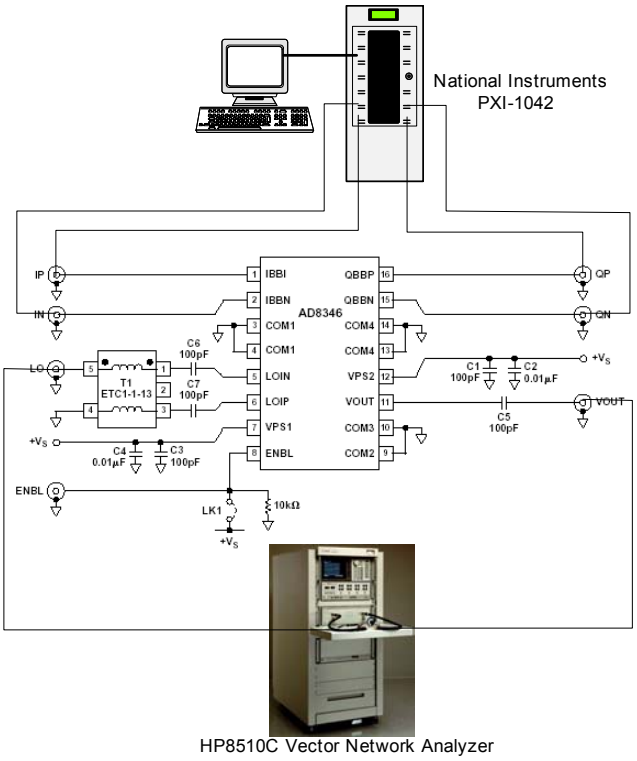

Figure 11. AD8346EVAL Bench Test Configuration.

The control voltages for the four input pins (i.e., IN, IP, QN and QP) of the AD8346EVAL board are supplied by the National Instruments PXI-1042, while a control program written in LabVIEW version 6.1 is used to control the amount of phase shift to the AD8346EVAL board. Figure 12 displays the AD8346EVAL cable connections while

Figure 13 shows a view of the control program Graphic User Interface (GUI) written in LabVIEW. In addition, Figure 14 shows the radar equipment cart containing the DSP (NI PXI-1042), the LO generator, and the multiple AD8346EVAL modulator boards.

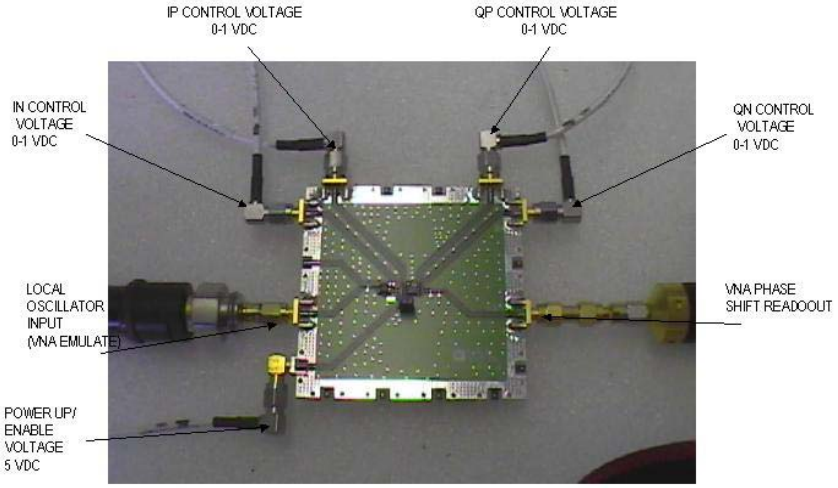

Figure 12. AD8346EVAL Cable and Signal Connections (From Ref. [3].).

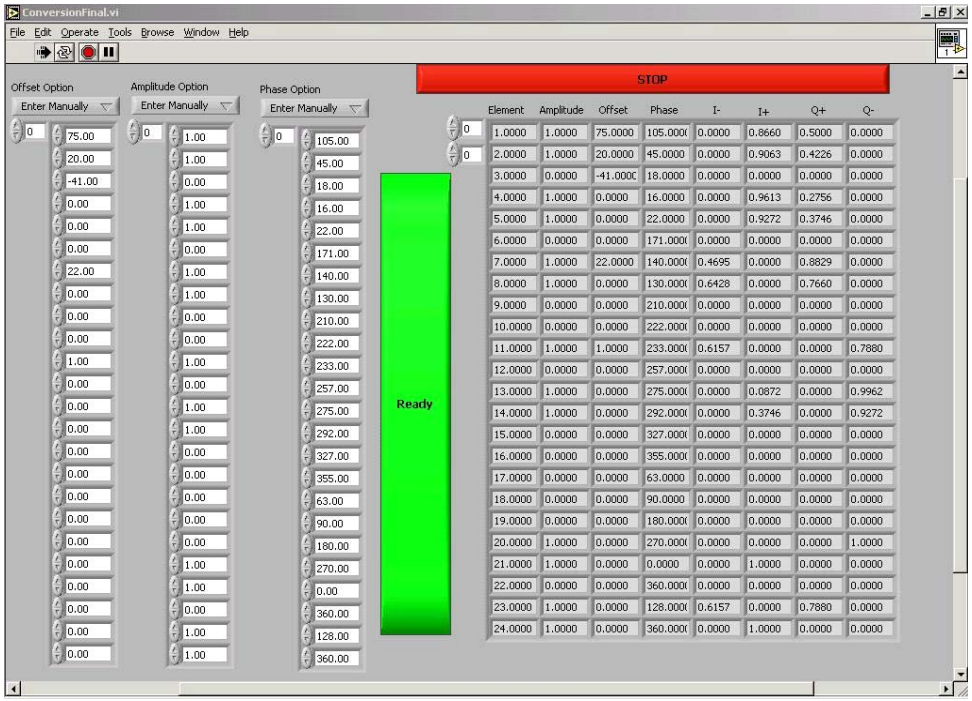

Figure 13. The Control Program GUI.

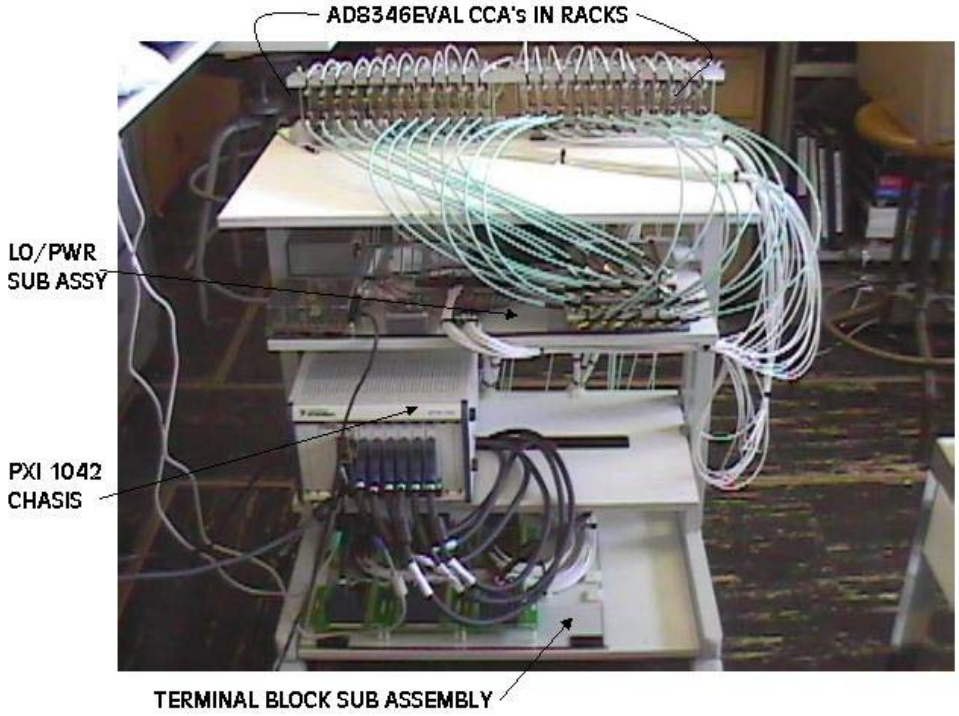

Figure 14. Radar Equipment Cart (From Ref. [3].).

One of the twenty-four inputs in the control program is used to set the voltage supply to the four input pins of the AD8346EVAL board for each element. The VNA supplies the local oscillator source signal and takes the measurements of the insertion phase shift and loss in the signal, as the control voltages are adjusted. The VNA is programmed to have a frequency sweep from 0.8 GHz to 2.5 GHz with an input power of 10 dBm. The S_{21} parameter for the AD8346EVAL board is then measured and saved. (The magnitude of S_{21} in dB is the insertion loss; the phase of S_{21} is the insertion phase.)

Figures 15 and 16 show the S_{21} parameter magnitude and phase measurements when the AD8346EVAL board is set to zero-phase by the control program.

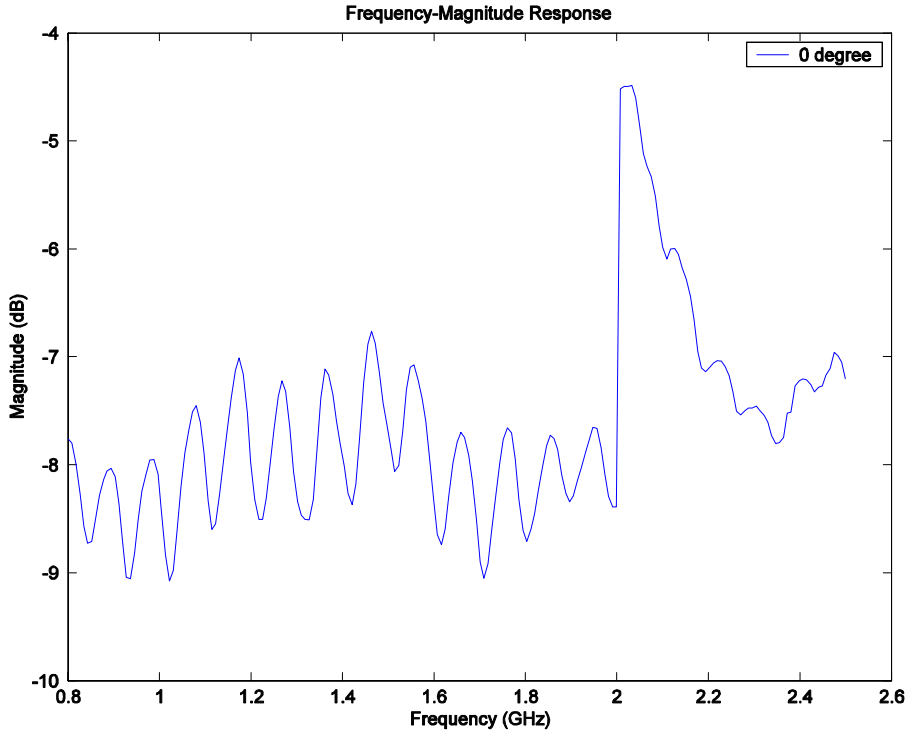

Figure 15. Frequency-Magnitude Response for Zero Phase Setting.

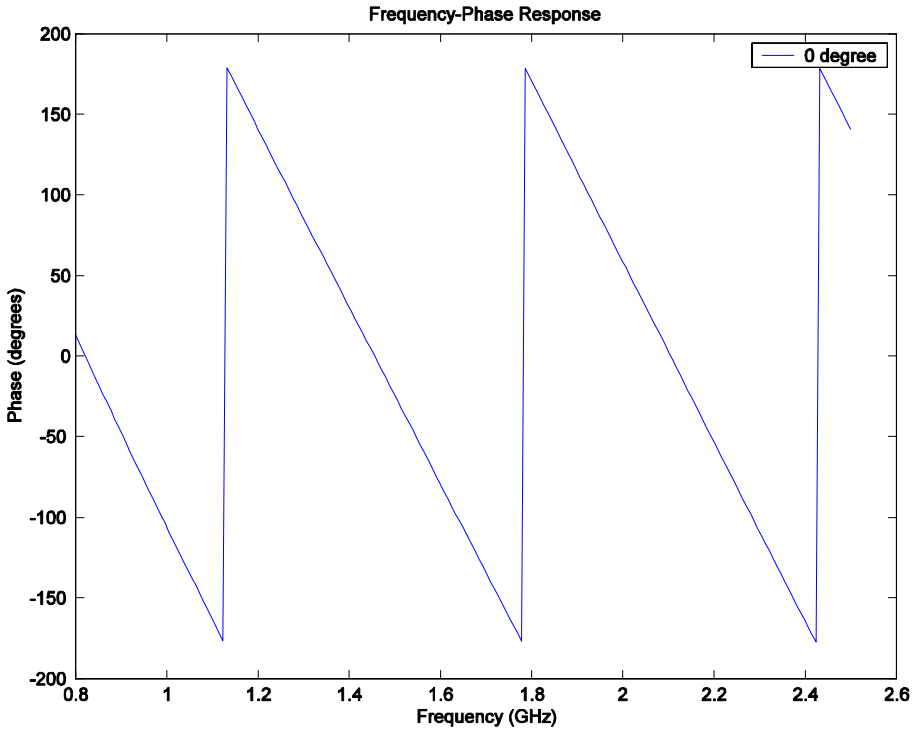

Figure 16. Frequency-Phase Response for Zero Phase setting.

Figure 15 shows that the AD8346EVAL board has an insertion loss that ranges from –6.5 dB to –9 dB in the frequency band from 0.8 GHz to 2 GHz. The magnitude increases to –4.5 dB from 2.0 GHz to 2.2 GHz. Figure 16 shows that the board has a linear phase slope from $-\pi$ to $+\pi$ radians. The calibration for the VNA was a direct connection, thus there are several cycles of phase as shown in the Figure 16. Note that the phase slope is negative, which is the opposite of what occurs for a passive device. A transmission line of length *d* has a phase given by $2\pi fd/c$, which has a positive phase slope.

The AD8346EVAL board is set for a 360° sweep in 1° increment and the S_{21} parameter measured at each 1° increment is saved. These measured data files are used for simulation of the array antennas in Chapter III, Section 4. The results of the measurements are plotted at 5° increments, in order to verify that the AD8346EVAL board phase slopes and magnitudes track as a function of phase state. Figures 17 to 20 show the results for phase shifts from 0° to 75°, 90° to 165°, 180° to 255°, and 270° to 345°, respectively. The modulo 360° phase measurements taken from the VNA are converted into linear continuous straight lines for ease of comparison. As expected, the phase shifts are observed to occur in sequence when the phase shift is changed sequentially from one value to another. For example, from Figure 17, the frequency-phase response at 30° phase shift is observed to be on top of the frequency-phase response at 15° phase shift. From the figures, it is clear that the frequency versus phase response of the AD8346EVAL board has a linear negative phase slope that tracks the phase shift settings.

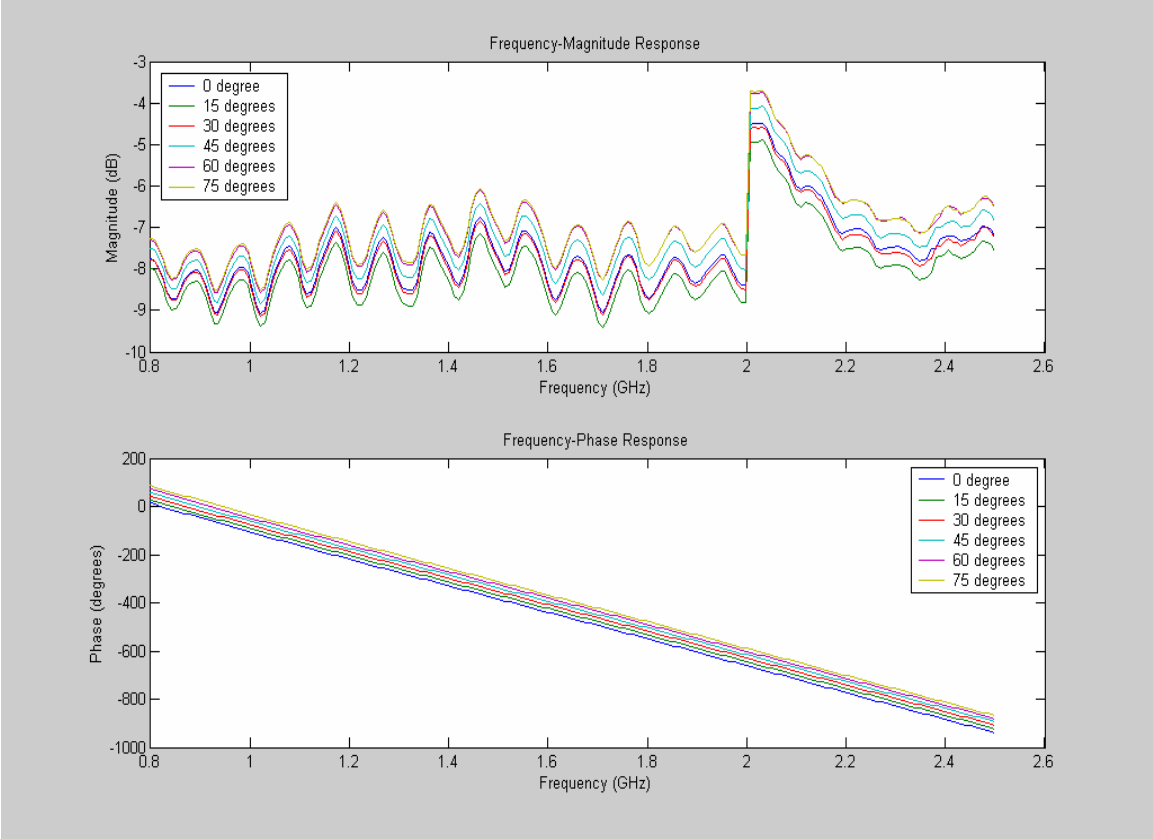

Figure 17. Magnitude and Phase Versus Frequency Response for Phase Shift From 0° to 75° at 5° Increments.

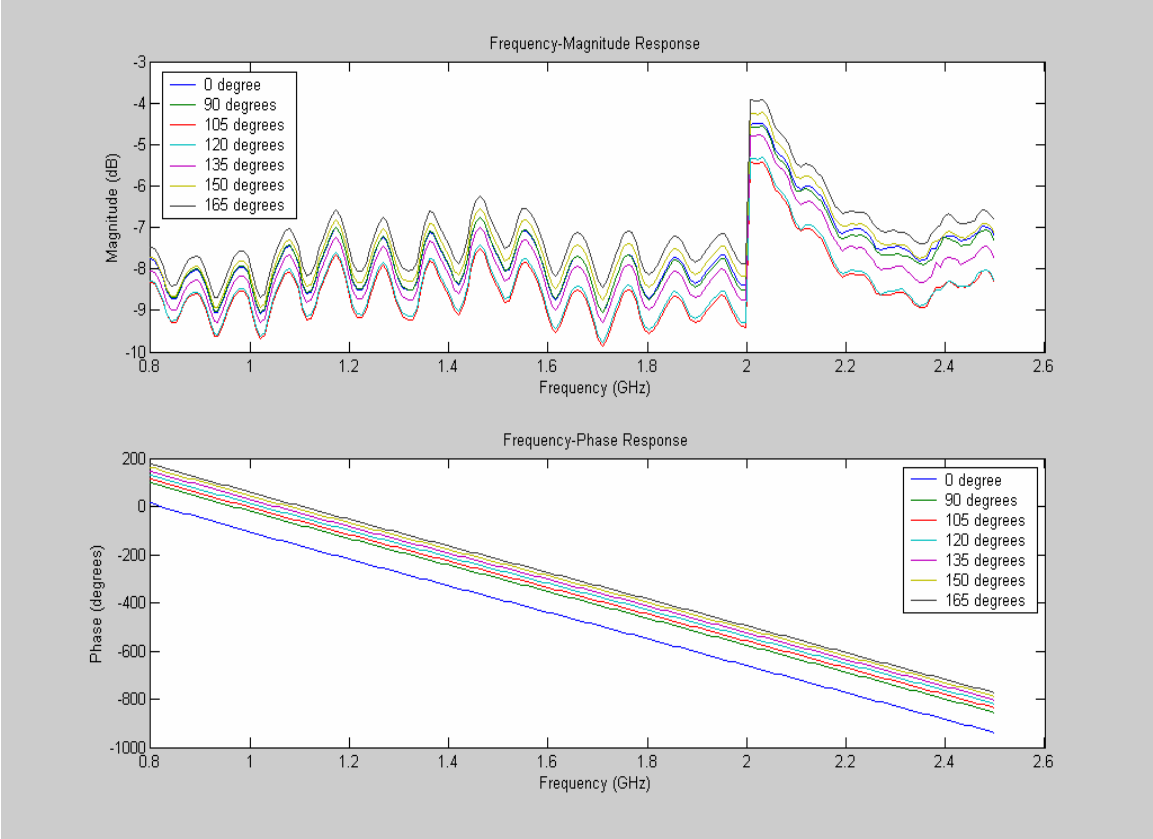

Figure 18. Magnitude and Phase Versus Frequency Response for Phase Shift From 90° to 165° at 5° Increments. (The 0° Phase Shift is Plotted for Reference.)

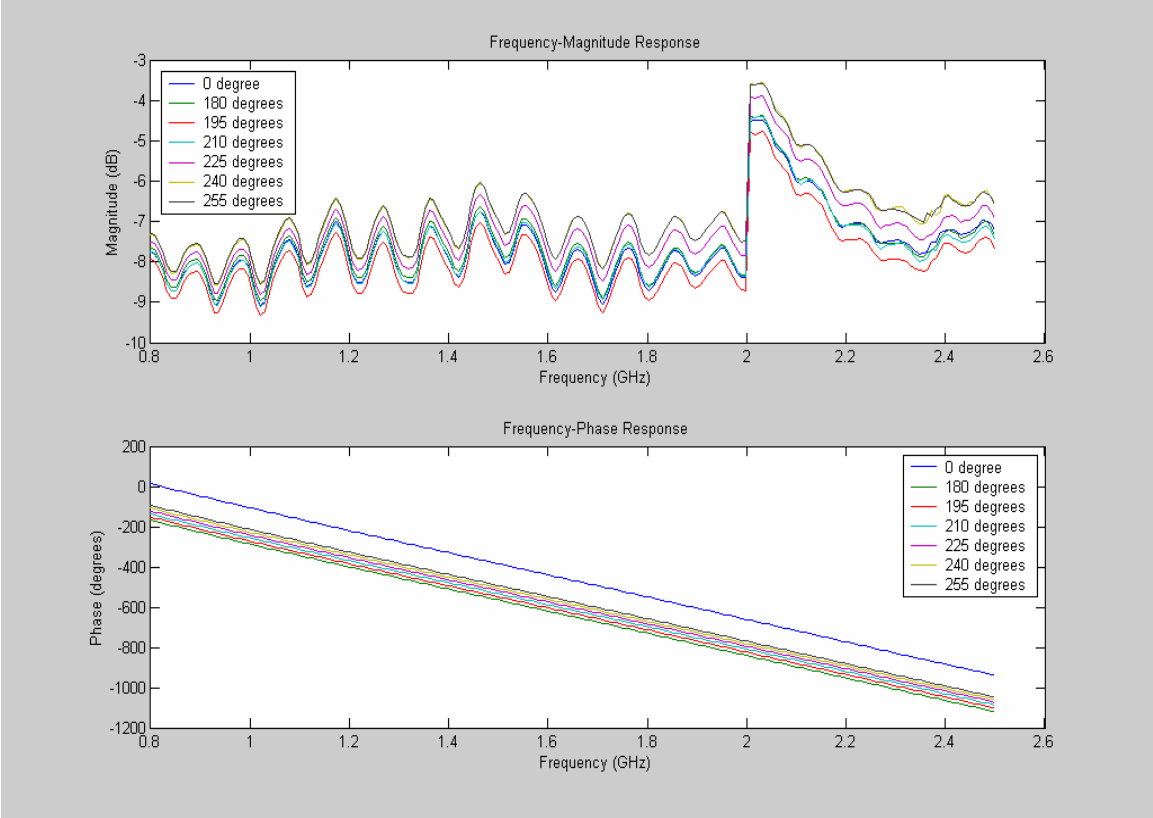

Figure 19. Magnitude and Phase Versus Frequency Response for Phase Shift From 180° to 255° at 5° Increments. (The 0° Phase Shift is Plotted for Reference.)

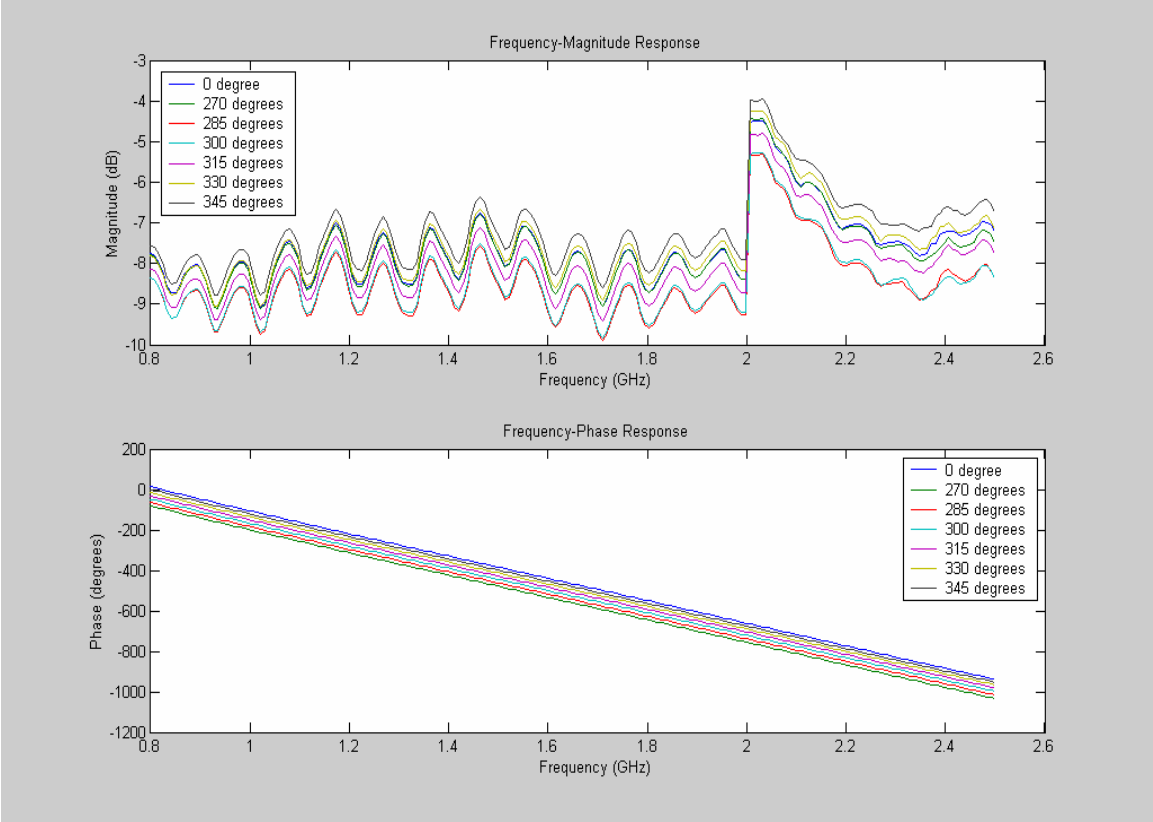

Figure 20. Magnitude and Phase Versus Frequency Response for Phase Shift From 270° to 345° at 5° Increments. (The 0° Phase Shift is Plotted for Reference.)

4. Implementation of a Linear Array

A simulation program was written to investigate whether the AD8346EVAL board is capable of providing wideband pattern characteristics, since the board has operating frequency from 0.8 GHz to 2.5 GHz. The simulation program was implemented in MathCAD and used the measured S_{21} parameters collected previously. A thirty-element linear array was considered and the radiation patterns at various operating frequencies were plotted for comparison.

a. Parameter Specifications

The simulation is based on the linear array shown in Figure 21. The physical spacing *d* between elements has to be fixed at a value that is based on a reference operating frequency. The reference frequency of 1.7 GHz is chosen in the middle of the operating frequency range of the AD8346EVAL board. Thus, the set of phase settings is computed at 1.7 GHz and held fixed for all frequencies. The operating parameters for the simulation program are as follows:

Number of elements, $N = 30$,

Reference frequency, $f_{ref} = 1.7$ GHz,

Reference wavelength, $\lambda_{ref} = c / f_{ref} = 0.176$ m,

Array spacing, $d = \lambda_{ref} / 2 = 0.088$ m,

The reference frequency wave number, $k_{ref} = 2\pi / \lambda_{ref} = 35.605$, and

The angle of transmission (scan angle), $\theta_s = 10^{\circ}$.

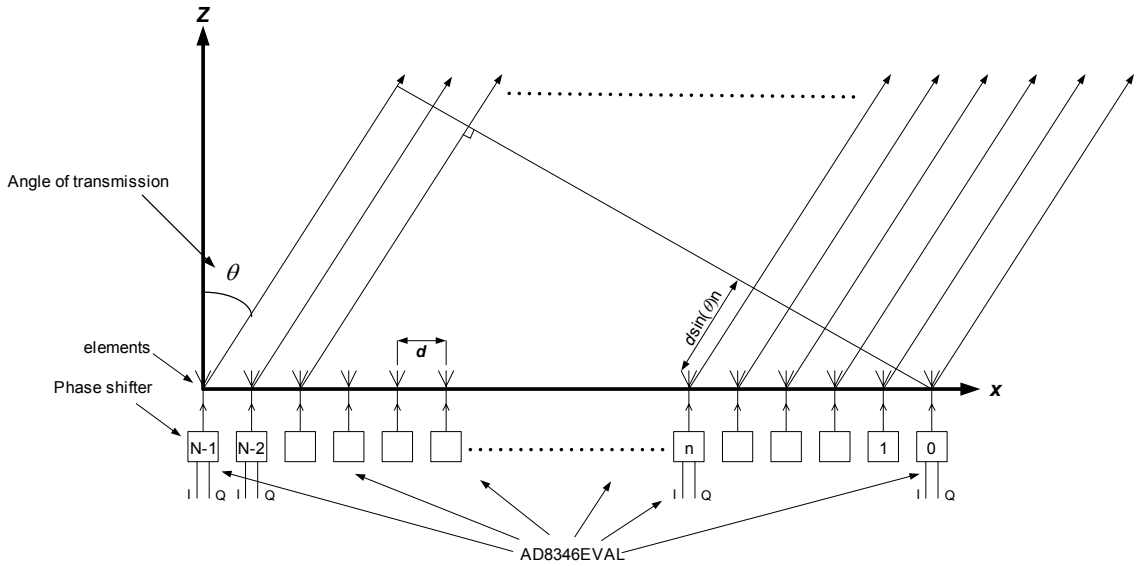

Figure 21. Thirty-Element Linear Array.

b. Phase Reference and Phase Shifts

Element 0 is chosen as the phase reference as shown in Figure 21. Based on this reference element, the phase shift setting at each element is given by Equation (14). The phase shift increment at element $n+1$ with respect to element n is

$$\begin{aligned} \Delta\Phi &= k_{ref}\, d \sin\theta_s \\ &= 35.605 \times 0.088 \times \sin(10°) \\ &= 31°. \end{aligned} \tag{14}$$

The phase shift associated with each element is shown in the Table 2.

Element	Phase Shift (°)	Element	Phase Shift (°)	Element	Phase Shift (°)
0	0	**10**	310	**20**	260
1	31	**11**	341	**21**	291
2	62	**12**	12	**22**	322
3	93	**13**	43	**23**	353
4	124	**14**	74	**24**	24
5	155	**15**	105	**25**	55
6	186	**16**	136	**26**	86
7	217	**17**	167	**27**	117
8	248	**18**	198	**28**	148
9	279	**19**	229	**29**	179

Table 2. Phase Shift Associated With Each Element.

The simulation program reads the corresponding measured data file based on the phase shifts listed in Table 2 for each element. For example, the 93° data file is read in for element 3. Figure 22 shows the Frequency-Phase and Frequency-Magnitude Responses for the 93° phase state. At any operating frequency, the corresponding phase and magnitude are read from the plot. For example, at $f_{oper} = 1.2$ GHz, the phase is $-130°$ and the magnitude is -7.1 dB. Hence, element 3 is set with phase $-130°$ and the amplitude at -7.1 dB for $f_{oper} = 1.2$ GHz. Therefore, the actual measured data are used in calculating the array factor at a given frequency.

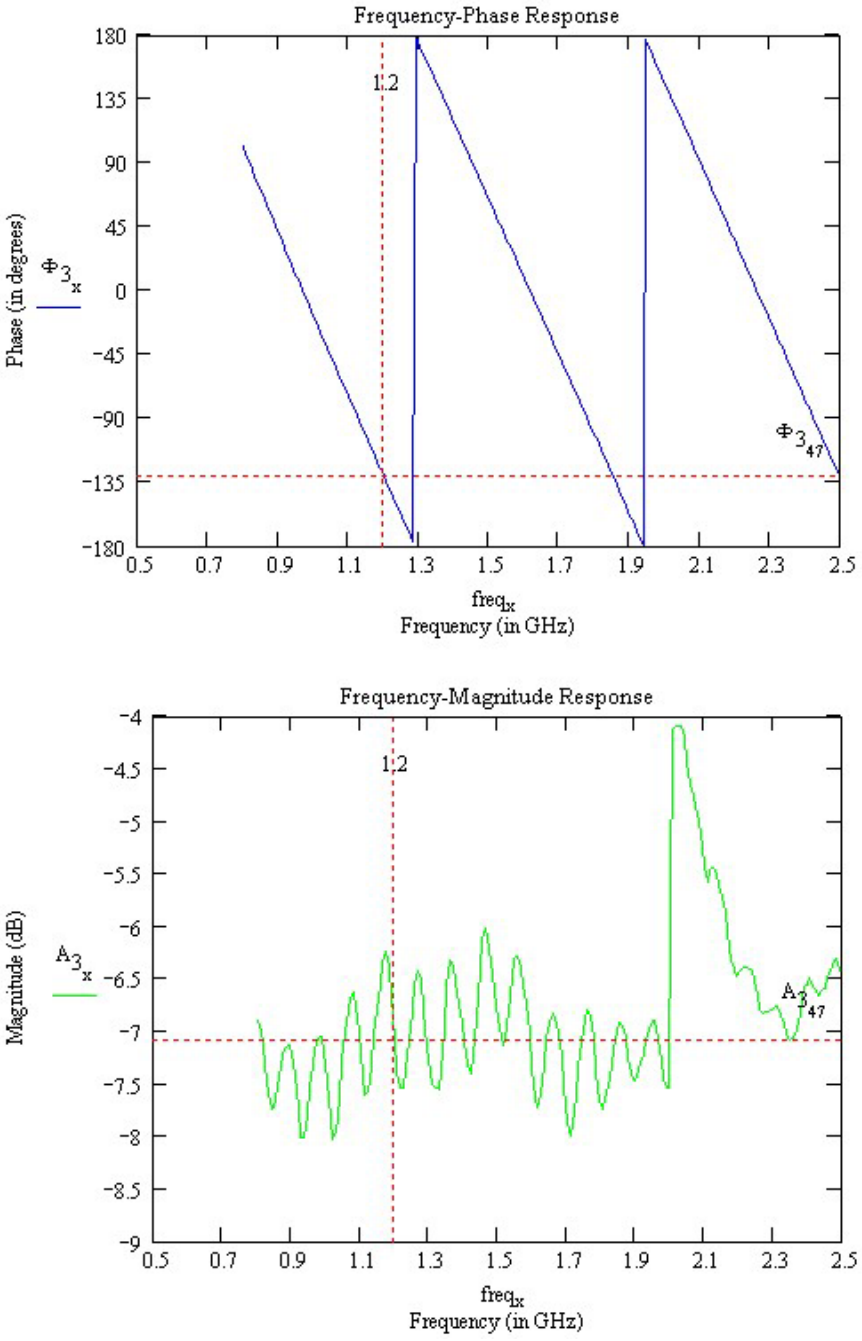

Figure 22. Frequency-Phase Response for a 93° Phase Shift Setting.

c. Radiation Patterns

With the calculated phase shift at each element, the program reads in the corresponding measured phase and amplitude data files for the AD8346EVAL board. Using Equation (1), the radiation pattern of a linear array at various operating frequencies

can be plotted. The radiation pattern for operating frequency $f_{oper} = 1.7$ GHz is shown in Figure 23.

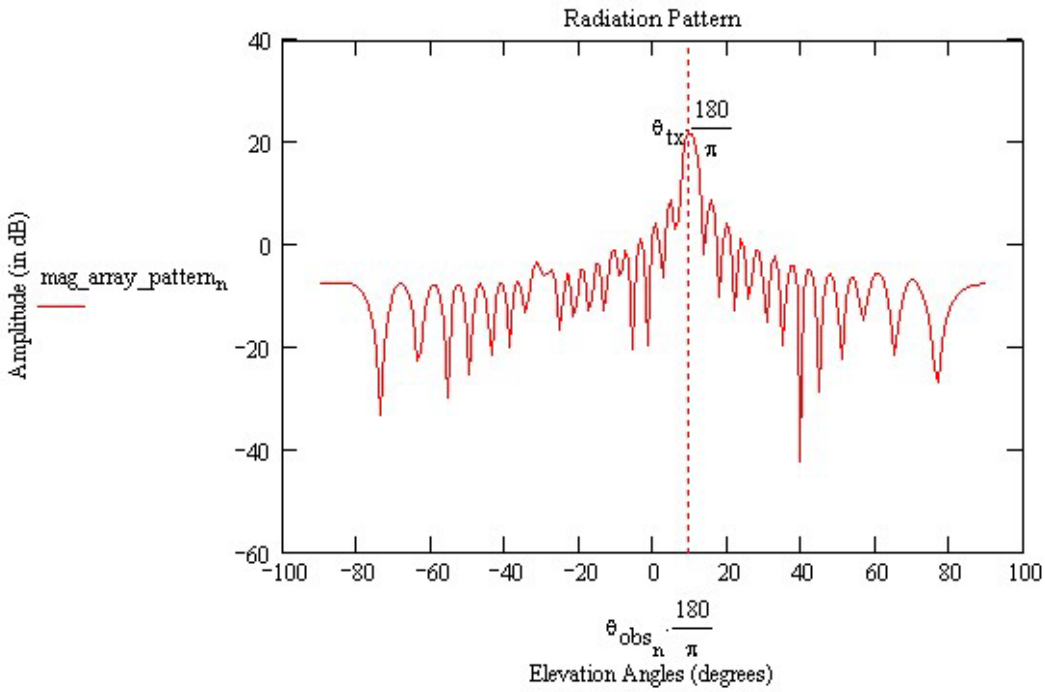

Figure 23. Radiation Pattern at $f_{oper} = 1.7$ GHz.

Figure 23 shows that the main beam of the linear array is scanned to the direction of transmission, i.e., $\theta_s = 10°$. However when the operating frequency is changed to 0.8 GHz, the mainbeam is squinted about +11° off of the direction of transmission, as shown in Figure 24. When the operating frequency is changed to 2.5 GHz, the mainbeam is squinted about −5° off of the direction of transmission as shown in Figure 25. Furthermore, because the phase slope of the modulator board is negative, the beam scans toward endfire as the frequency is decreased. This is the opposite of what would occur if a passive beamforming network is used.

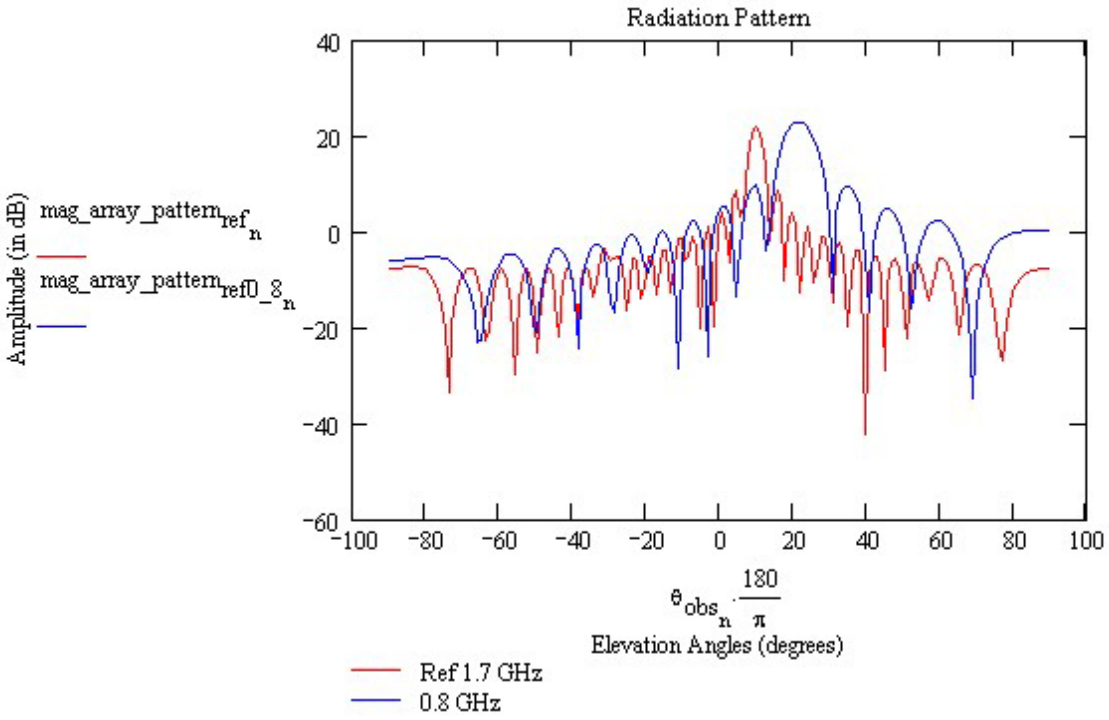

Figure 24. Radiation Pattern at $f_{oper} = 0.8$ GHz Compared to $f_{ref} = 1.7$ GHz.

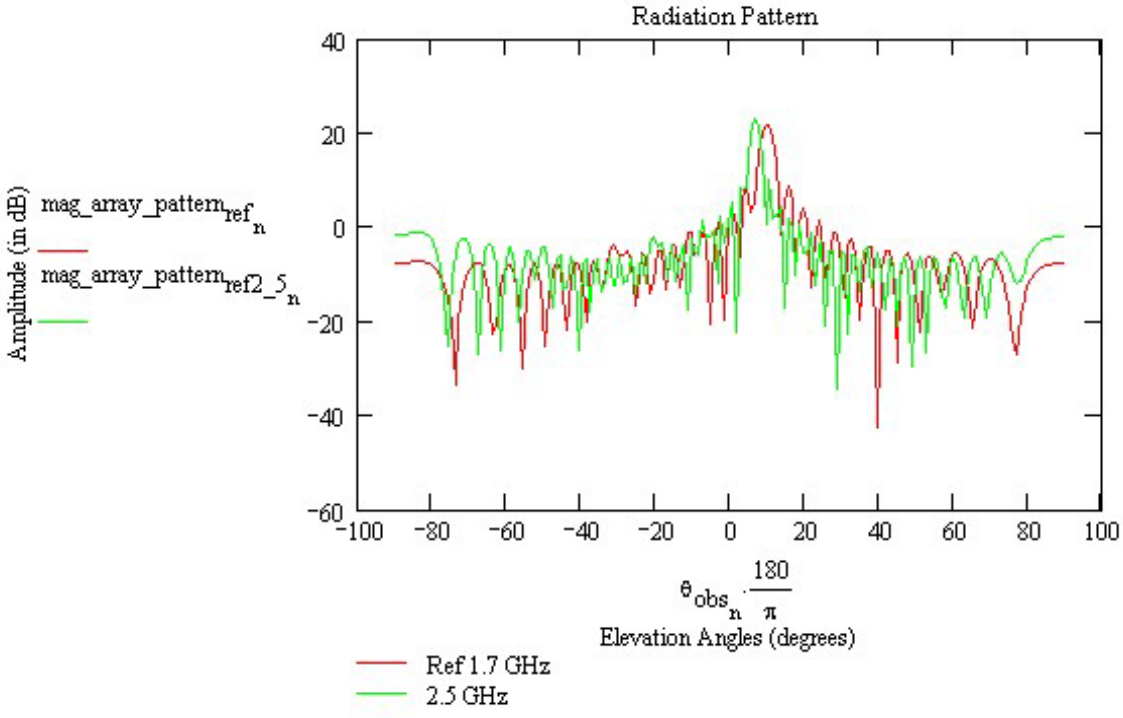

Figure 25. Radiation Pattern at $f_{oper} = 2.5$ GHz Compared to $f_{ref} = 1.7$ GHz.

The half-power beamwidth of the radiation pattern changes according to [16]

$$\theta_B \approx \frac{0.866c}{Ndf_{oper}\cos(\theta_s)}. \tag{15}$$

Thus, the beamwidth of the radiation patterns are broader (i.e., see Figure 24) and narrower (i.e., see Figure 25) when the operating frequencies are 0.8 GHz and 2.5 GHz, respectively. As evident from radiation patterns, the AD8346EVAL board does not have a wide instantaneous bandwidth characteristic. If the transmitted waveform has frequency components between 0.8 and 2.5 GHz, then the low frequencies are radiated in a different direction than the high frequencies.

B. PHASED ARRAY RECEIVER

The next phase of the project was to develop a complementary receive array. This would allow the GA to be verified for the entire beam forming process from transmitting to reception. Three approaches were considered in developing a receive digital phased array. These options are described in the following paragraphs.

1. Receiver Component Design Considerations

a. Option One

In option one, twenty-four RF Signal Analyzers from National Instruments (NI) are considered, with each an RF Signal Analyzer feeding to one antenna element of the twenty-four elements used in the array receiver, as shown in Figure 26.

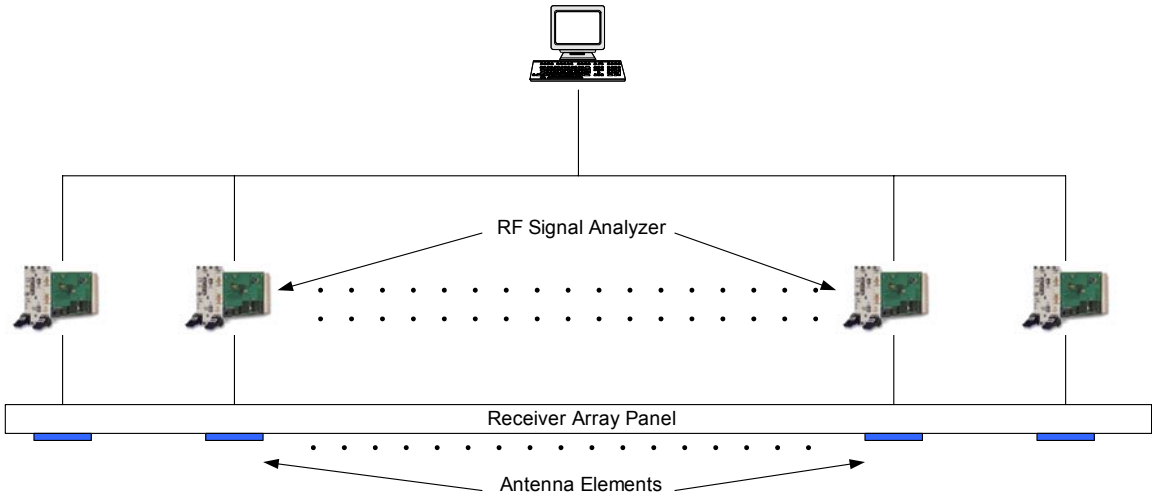

Figure 26. Option One for Array Receiver.

The RF Signal Analyzer is readily available and the software program to be written in LabVIEW program will be compatible with the 3-D 2.4-GHz Phased Array Transmit Antenna. However this is a very costly solution because the RF signal analyzer is a high cost item ($11,000 each).

b. Option Two

In option two, two of the RF Signal Analyzers proposed in option one are used, each controlling three National Instruments ADCs switches as shown in Figure 27.

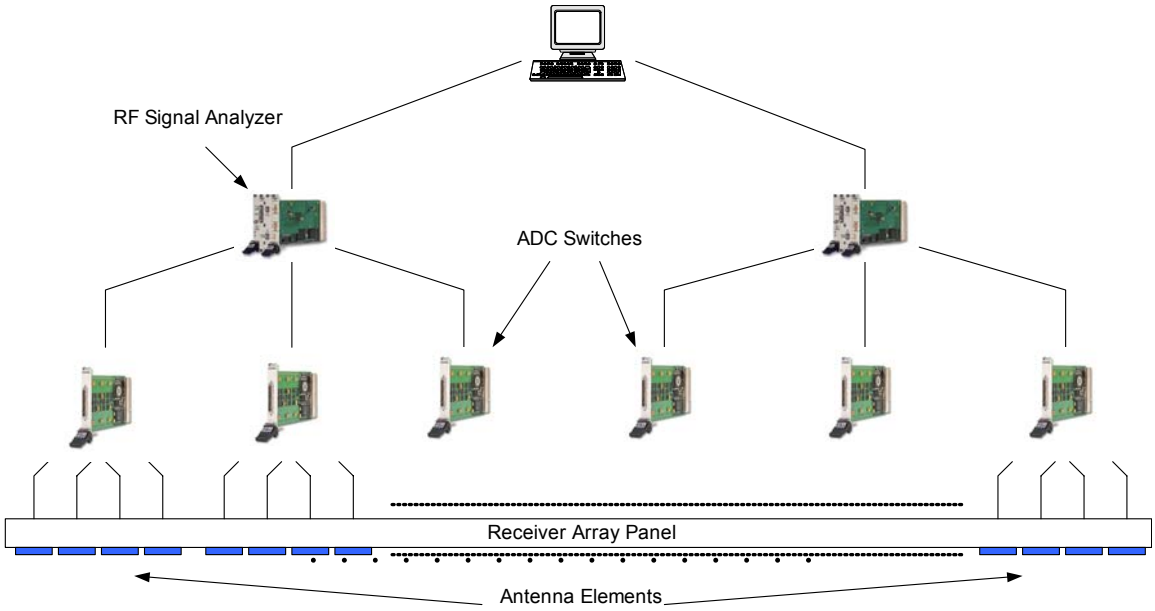

Figure 27. Option Two for Array Antenna.

There are six NI ADCs used in the architecture of the array receiver. Each ADC controls four antenna elements of the twenty-four antenna elements in the array. Although this option is cheaper than option one, it is still too costly due to the use of the RF Signal Analyzers.

c. Option Three

In option three, COTS I/Q demodulator boards performing as phase shifters is proposed. As shown in Figure 28, each of the demodulator boards feeds one antenna element. The output of the demodulator card is connected to a COTS DAC, which in turn is connected to a NI low-cost Input/Output (I/O) board. These I/O boards will be controlled by one RF Signal Analyzer.

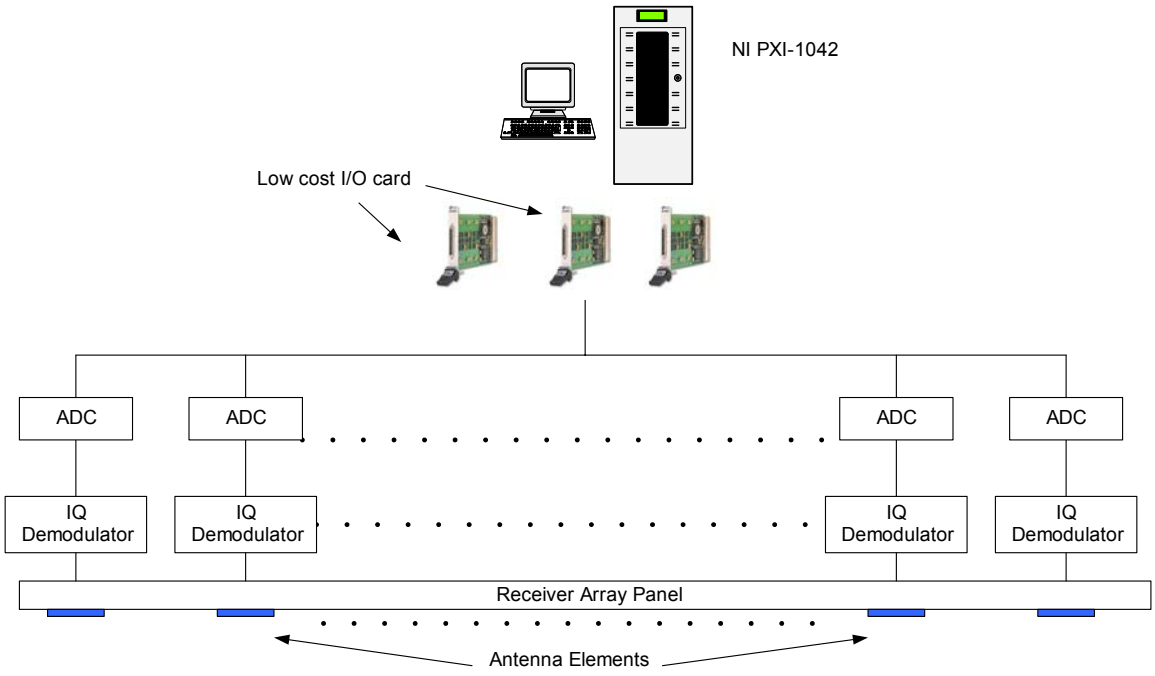

Figure 28. Option Three for Array Antenna.

The cost of the demodulator is one hundred dollars while the DAC cost about two hundred dollars. Thus option three is considered the cheapest among the three options. However, these demodulators have to be verified as to whether they can perform as phase shifters in the receive array antenna.

The AD AD8347EVAL Quadrature Demodulator board was selected as a possible candidate for the phase shifter. The AD8347EVAL board is the receive version of the AD8346EVAL board used in the 3-D 2.4 GHz Phased Array Transmit Antenna.

2. AD8347EVAL Quadrature Demodulator

The AD8347EVAL board is a silicon RFIC broadband direct quadrature demodulator with RF and baseband Automatic Gain Control (AGC) amplifiers. It is fully complementary with the AD8346EVAL modulator board for use in many communications receivers, performing quadrature demodulation directly to baseband frequencies. Figure 29 shows the electrical schematic of the AD8347EVAL microcircuit.

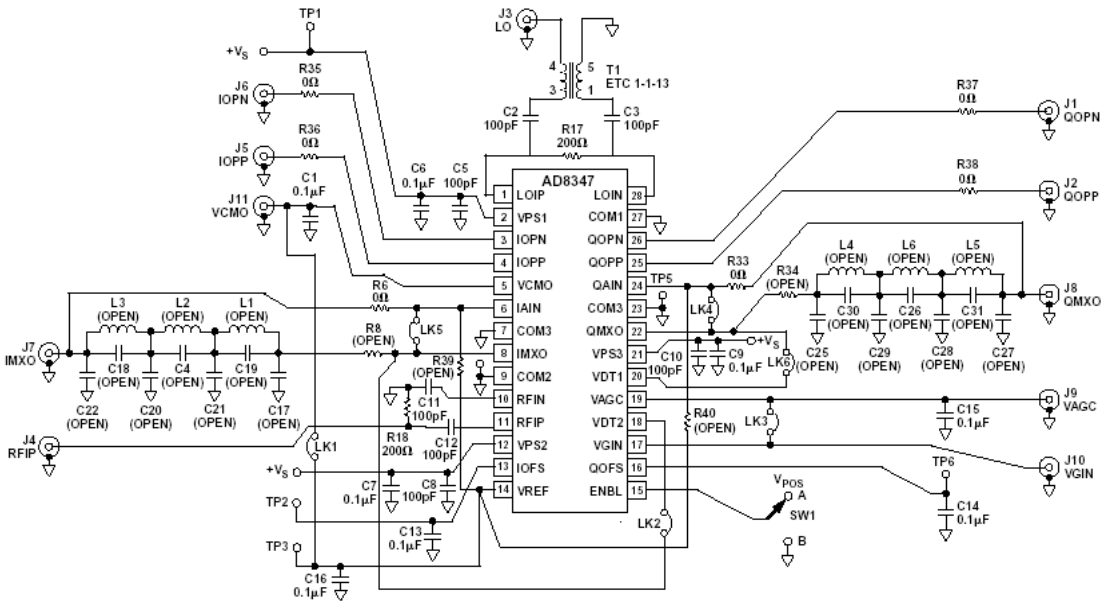

Figure 29. AD8347EVAL Circuit Diagram (From Ref. [17].).

The AD8347EVAL board RF input frequency ranges from 0.8 GHz to 2.7 GHz and the baseband outputs can be connected directly to an ADC. The RF signal is directly down converted to the baseband *I* and *Q* components using a LO signal at the same frequency as the RF signal. Direct conversion RF receiver architecture promises superior performances in power, size and cost over that of a superheterodyne based receiver [18].

There are thirteen signals lines in the form of SMA connectors in the AD8347EVAL board of which six signals are used in the bench test configuration described in Section 3. There are the Radio Frequency Input Positive (RFIP), Local Oscillation (LO), In-phase Output Pin Negative (IOPN), In-phase Output Pin Positive (IOPP), Quadrature Output Pin Negative (QOPN) and Quadrature Output Pin Positive (QOPP).

The RFIP and LO signal lines are configured for single-ended connections while the baseband outputs (IOPN, IOPP, QOPN, and QOPP) are configured for differential connections. The rest of the SMA connectors are mainly used for monitoring of the AD8347EVAL board.

3. AD8347EVAL Quadrature Demodulator Bench Test Configuration

A bench test was setup to investigate the operating characteristics of the AD8347EVAL board. The bench test configuration is shown in Figure 30.

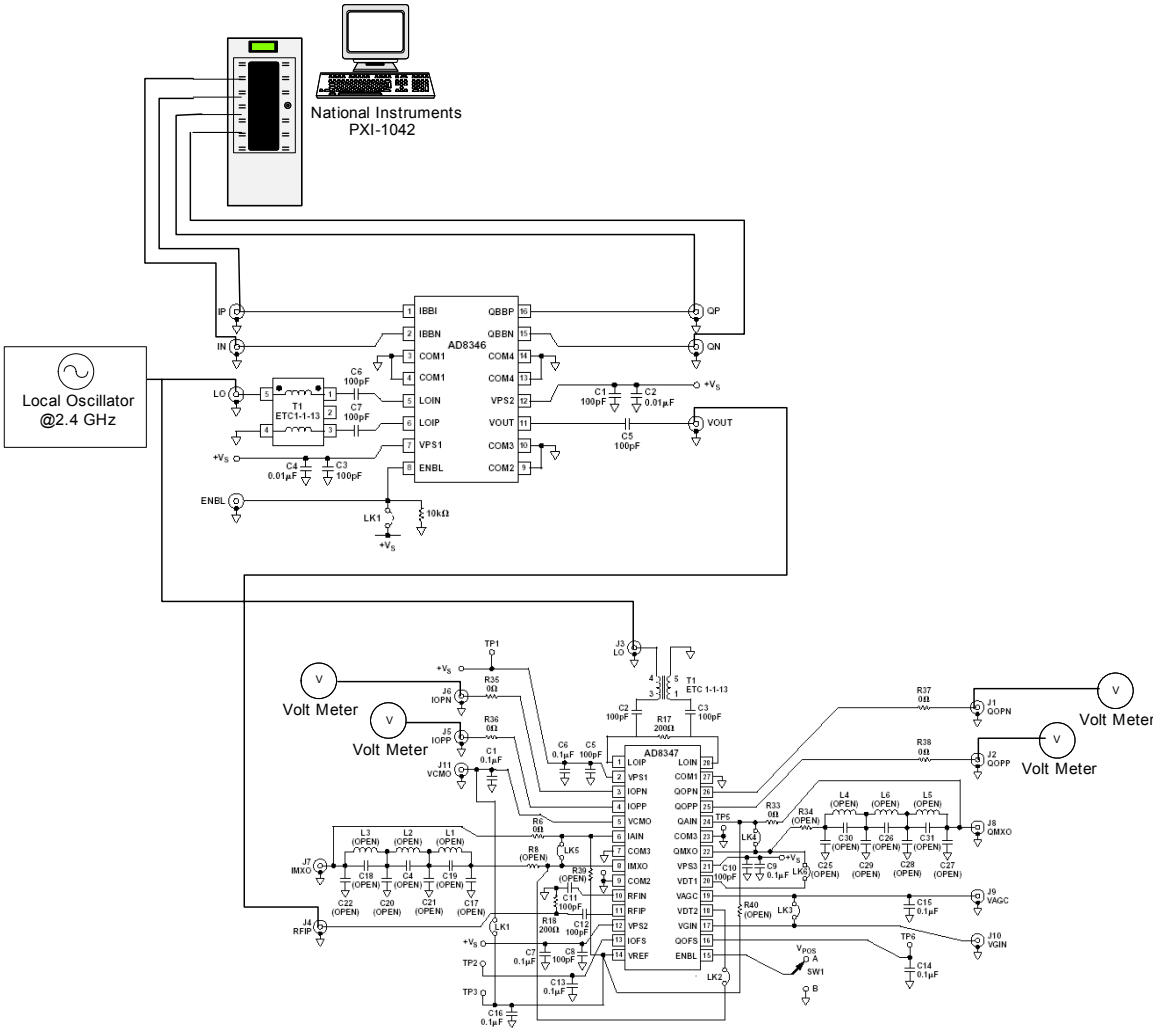

Figure 30. AD8347EVAL Bench Test Configuration.

A 5 VDC is supplied to the AD8347EVAL board by an external dc power supply. The positive and negative voltages of the dc power supply are connected to the pins "VS" and "GND" as shown in Figure 31. The location of the power ON/OFF switch is shown in Figure 31 as well. One of the AD8346EVAL transmit boards supplied the phase shifted RF signal to the RFIP of the AD8347EVAL board. The same LO generator operating at 2.4 GHz, used in the transmit antenna, is also used to supply the LO signal to the AD8347EVAL board. Hence the received RF signal is perfectly synchronized with

the LO signal at the AD8347EVAL board. The connections for the RF and LO signals can be seen in Figure 31. According to Reference 17, the operating range of the LO signal is between −10 and 0 dBm, whereas the signal supply by the LO generator is 12 dBm. Thus a RF attenuator (19 dB) has to be connected to the LO of the AD8347EVAL board before connecting the signal from the LO generator.

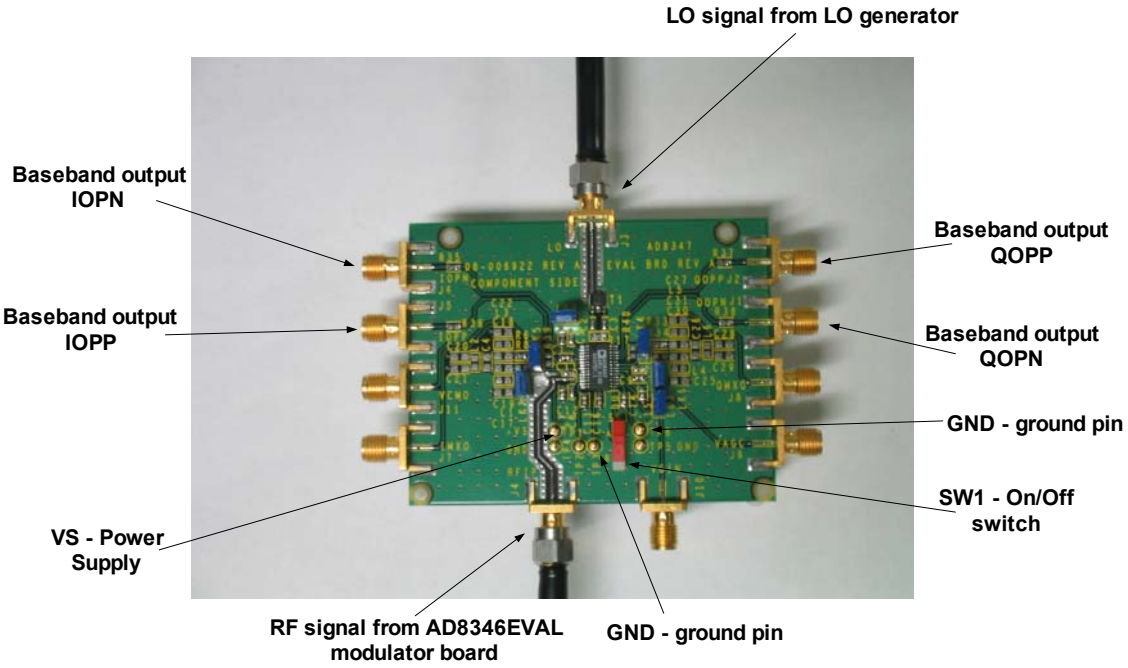

Figure 31. AD8347EVAL Cable/Signal Connections.

The LabVIEW control program is used generate the amplitude and phase of the RF output signal from the AD8346EVAL board. This RF signal is then sent to the RFIP of the AD8347EVAL board, as shown in Figure 31. Finally, the baseband output signals (IOPP, IOPN, QOPP and QOPN) are measured with respect to ground using a digital multi-meter.

4. Experimental Measurements

The test bench is configured for a 360° sweep in 5° increments using the LabVIEW control program. The results of the measured baseband output values are tabulated in Table 3.

TRANSMIT PHASE (°)	IOPP (VDC) VOLTAGE	IOPN (VDC) VOLTAGE	QOPP (VDC) VOLTAGE	QOPN (VDC) VOLTAGE
0	1.0388	0.9907	1.1180	0.9105
5	1.0340	0.9958	1.1165	0.9120
10	1.0290	1.008	1.1144	0.9141
15	1.0232	1.0068	1.1114	0.9169
20	1.0165	1.0135	1.1076	0.9208
25	1.0015	1.0292	1.0979	0.9306
30	0.9450	1.0865	1.0420	0.9864
35	0.9248	1.1066	1.0028	1.0244
40	0.9213	1.1097	0.9956	1.0315
45	0.9193	1.1118	0.9908	1.0362
50	0.9181	1.1134	0.9869	1.0398
55	0.9169	1.1145	0.9831	1.0435
60	0.9159	1.1154	0.9797	1.0468
65	0.9152	1.1162	0.9768	1.0497
70	0.9146	1.1168	0.9733	1.0529
75	0.9142	1.1172	0.9702	1.0562
80	0.9139	1.1175	0.9676	1.0591
85	0.9136	1.1178	0.9642	1.0619
90	0.9134	1.1180	0.9605	1.0657
95	0.9136	1.1178	0.9563	1.0700
100	0.9142	1.1172	0.9513	1.0748

Table 3. Results of AD8347EVAL Bench Test.

TRANSMIT PHASE (°)	IOPP (VDC) VOLTAGE	IOPN (VDC) VOLTAGE	QOPP (VDC) VOLTAGE	QOPN (VDC) VOLTAGE
105	0.9153	1.1162	0.9465	1.0797
110	0.9172	1.1143	0.9399	1.0863
115	0.9247	1.1069	0.9131	1.1141
120	0.9815	1.0489	0.8322	1.1929
125	1.0107	1.0194	0.8138	1.2109
130	1.0174	1.0123	0.8096	1.2152
135	1.0218	1.0081	0.8070	1.2181
140	1.0255	1.0041	0.8048	1.2199
145	1.0292	1.0005	0.8026	1.2216
150	1.0320	0.9975	0.8011	1.2233
155	1.0351	0.9943	0.7998	1.2246
160	1.0383	0.9912	0.7990	1.2257
165	1.0407	0.9887	0.7980	1.2267
170	1.0436	0.9858	0.7972	1.2276
175	1.0466	0.9827	0.7962	1.2284
180	1.0496	0.9795	0.7954	1.2291
185	1.0541	0.9751	0.7948	1.2295
190	1.0587	0.9705	0.7944	1.2298
195	1.0631	0.9660	0.7946	1.2297
200	1.0688	0.9602	0.7953	1.2295
205	1.0866	0.9420	0.7972	1.2275
210	1.1898	0.8375	0.8508	1.1743
215	1.2355	0.7914	0.9218	1.1039
220	1.2405	0.7863	0.9390	1.0877
225	1.2422	0.7845	0.9437	1.0823
230	1.2433	0.7835	0.9473	1.0791

Table 3 (Continued). Results of AD8347EVAL Bench Test.

TRANSMIT PHASE (°)	IOPP (VDC) VOLTAGE	IOPN (VDC) VOLTAGE	QOPP (VDC) VOLTAGE	QOPN (VDC) VOLTAGE
235	1.2441	0.7826	0.9503	1.0760
240	1.2446	0.7820	0.9534	1.0728
245	1.2451	0.7815	0.9565	1.0697
250	1.2455	0.7811	0.9595	1.0671
255	1.2457	0.7809	0.9618	1.0643
260	1.2458	0.7806	0.9646	1.0616
265	1.2459	0.7807	0.9678	1.0588
270	1.2458	0.7806	0.9706	1.0557
275	1.2454	0.7811	0.9750	1.0512
280	1.2445	0.7821	0.9793	1.0471
285	1.2431	0.7836	0.9843	1.0419
290	1.2409	0.7858	0.9897	1.0367
295	1.2374	0.7896	0.9981	1.0290
300	1.2234	0.8037	1.0280	0.9977
305	1.1307	0.8986	1.1105	0.9160
310	1.0771	0.9523	1.1217	0.9069
315	1.0688	0.9603	1.1223	0.9063
320	1.0647	0.9645	1.1226	0.9060
325	1.0610	0.9684	1.1224	0.9059
330	1.0578	0.9714	1.1223	0.9060
335	1.0546	0.9748	1.1219	0.9064
340	1.0511	0.9781	1.1214	0.9069
345	1.0486	0.9807	1.1210	0.9073
350	1.0452	0.9841	1.1202	0.9080
355	1.0421	0.9872	1.1195	0.9086

Table 3 (Continued). Results of AD8347EVAL Bench Test.

After measuring the four baseband outputs, the next step is to calculate the differential voltages for *I* and *Q*, and then use Equation (13) to plot the received phase and compare it with the transmitted phase. The expected waveform should be a straight line with a slope of +1. A MATLAB program was written to plot and analyze the measured data.

The measured differential *I* and *Q* components are plotted against the transmitted phase and are shown in Figure 32. Ideally, the *I* and *Q* signals should be sinusoidal waveforms with zero dc level. The plotted *I* and *Q* signals resemble cosine and sine waves, respectively, but they have dc shift and their phases are offset. A manually derived dc offset value was introduced to the *I* and *Q* signal to bring the dc level to zero, and the result is also shown in Figure 32. The dc level of the *I* and *Q* signals were probably due to phase error in the transmitted RF signal from the AD8346EVAL board.

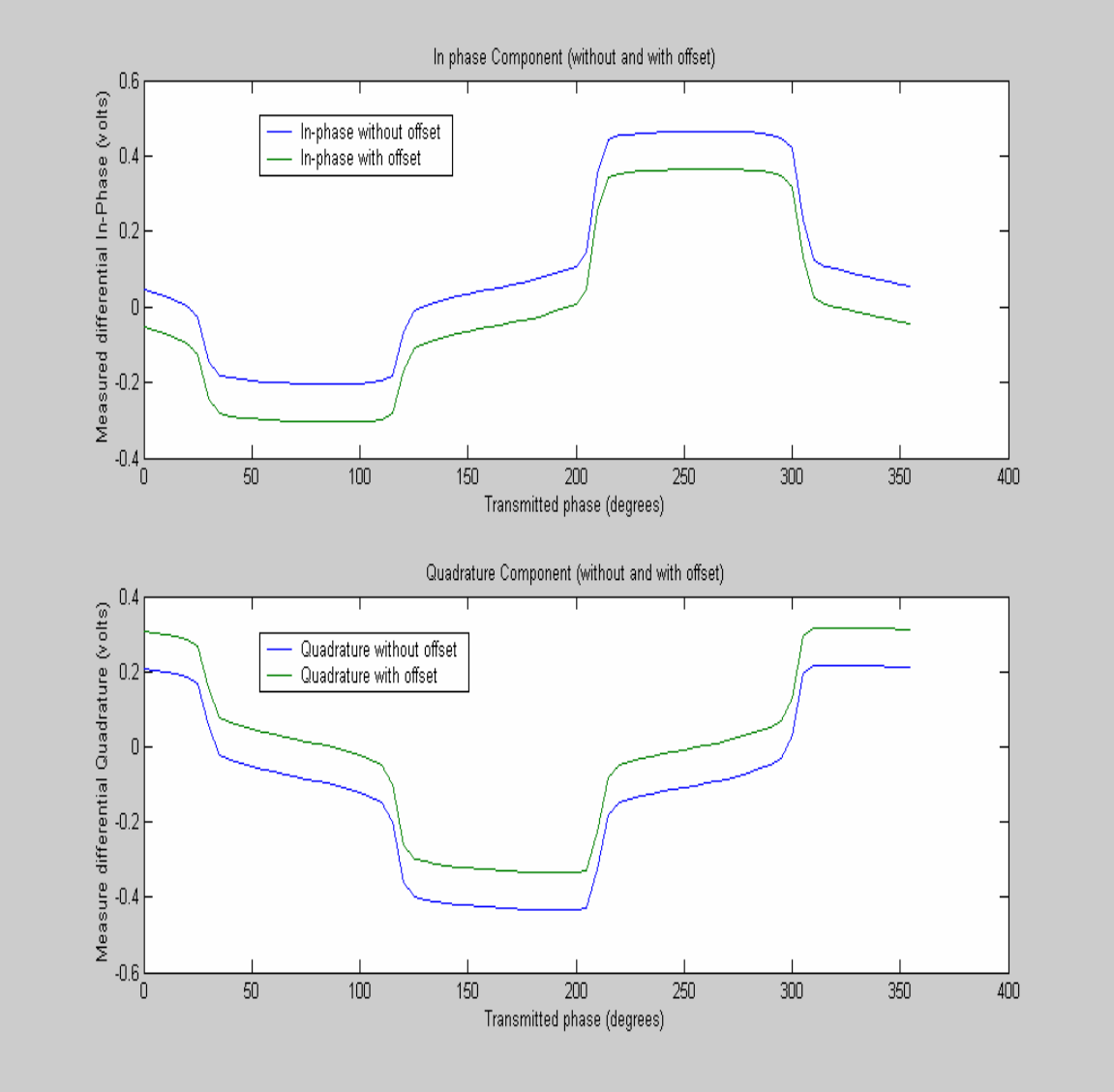

Figure 32. Measured Differential *I* and *Q* Components Without and With Offsets.

Figure 33 shows that the *I* and *Q* signals exhibit characteristics similar to the cosine and sine waveform, respectively, but with some phase offsets. A phase offset is not of concern, since any offset in the transmitted signal would be present in all elements of the array. Only the phase progression (differences in phase) affects the receive array output.

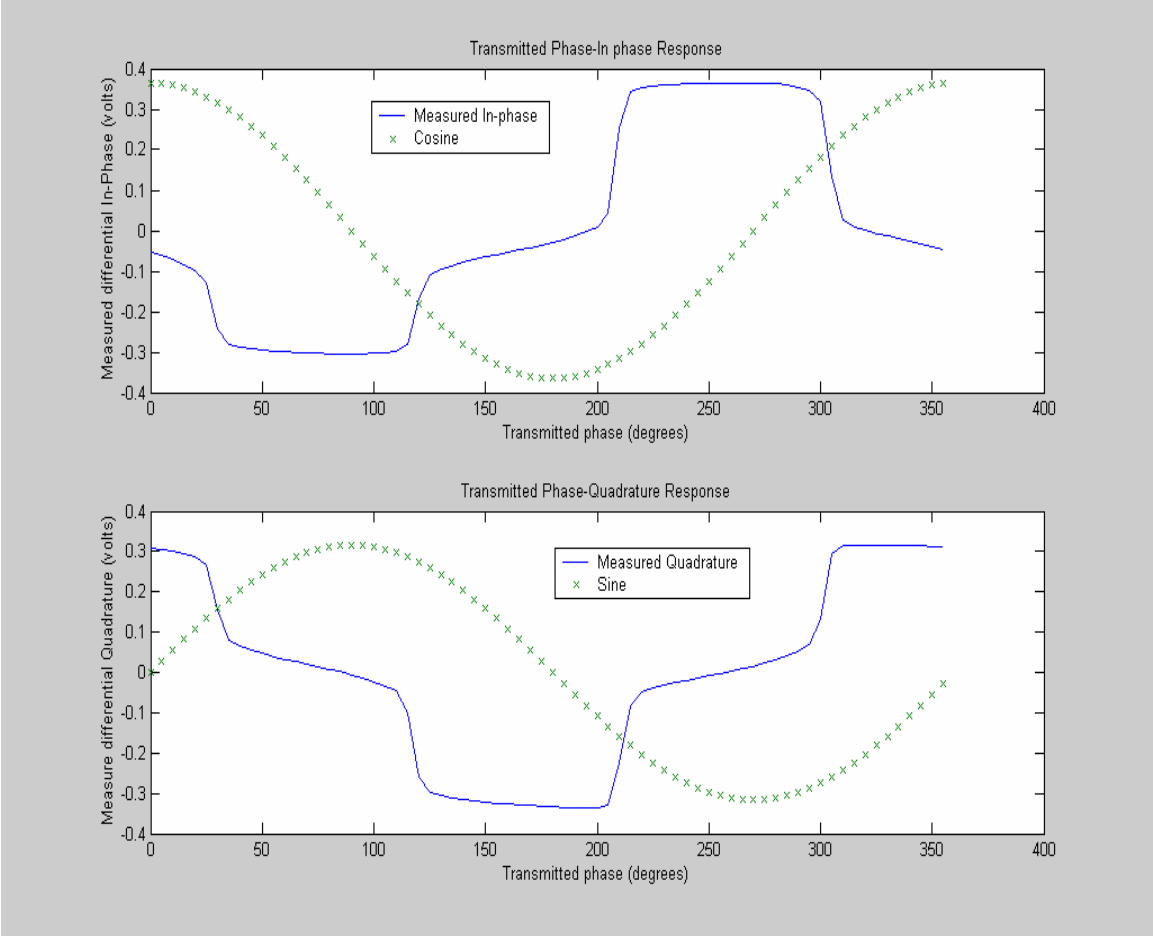

Figure 33. Measured Differential *I* and *Q* Components Versus Transmitted Phase Response.

Figure 34 shows the Transmitted Phase versus Measured Phase response of the AD8347EVAL board. The measured phase is fairly linear, but with some ripples. The ripples represent phase error. The ripple is due to measurement error and phase errors that occur in both the modulator used for the transmitting the signal, and the demodulator circuit. Esswein's measurements [3] showed that the modulator phase errors were greatest in the diagonals of the *I*-*Q* plane. For example, if the controlling software commands the modulator to a 45° phase shift, the actual phase shift might be 49.3°. This type of phase error is greatest at 45°, 135°, 225°, and 315°, which fits the period of the ripple in Figure 34.

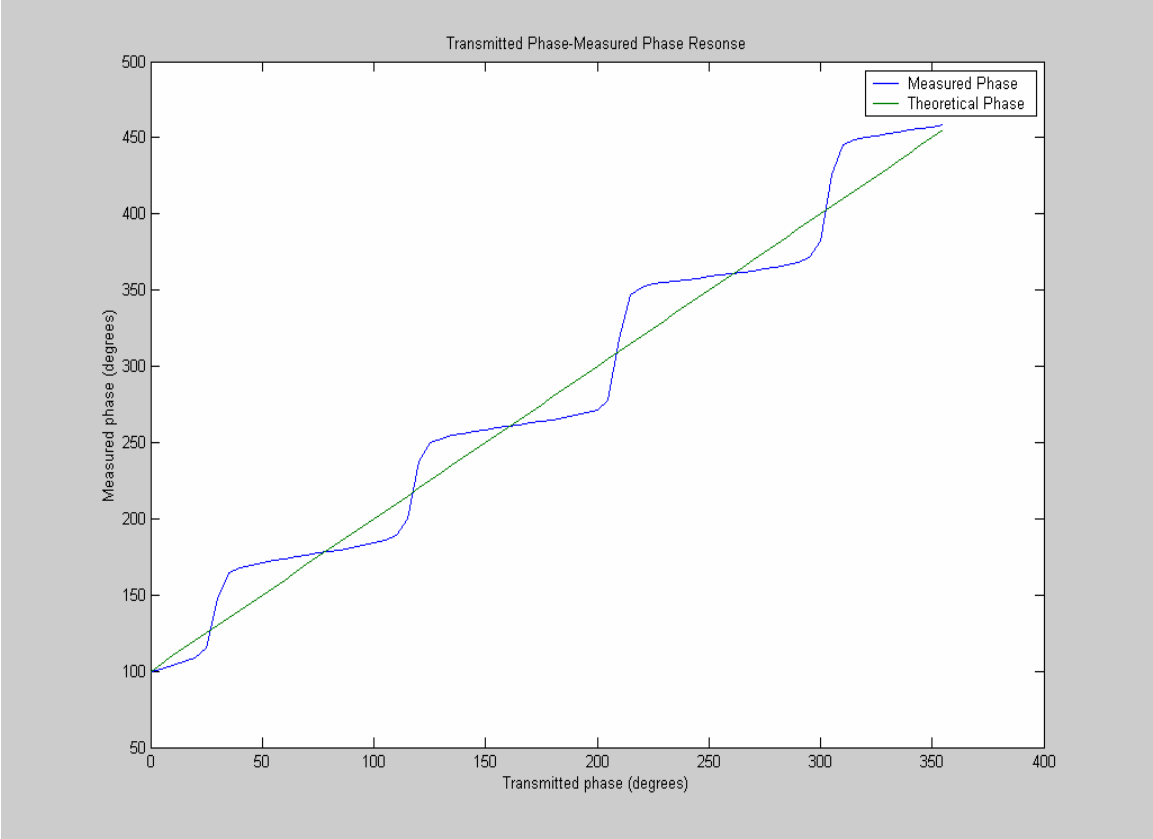

Figure 34. Transmitted Phase Versus Measured Phase Response.

C. SUMMARY

This chapter has presented the experimental setups of the AD8346EVAL modulator and AD8347EVAL demodulator boards. The results of the modulator board obtained from the experiment are incorporated into the simulation of a linear array and the resulted radiation patterns from the simulation showed that the modulator board does not have a wide instantaneous bandwidth characteristic. Also, the results of the demodulator board obtained from the experiment indicated that the board works successfully as a phase shifter.

THIS PAGE INTENTIONALLY LEFT BLANK

IV. CONCLUSIONS AND RECOMMENDATIONS

A. SUMMARY

Digital antennas have the potential of satisfying the requirements of many systems simultaneously. They are flexible, and capable of handling wide bandwidths, and can perform multiple functions. The bandwidth of the modulator and demodulator must match the bandwidth of the signal for efficient operation. Measurements on the AD8346EVAL transmit modulator revealed the instantaneous bandwidth is much narrower than the specified frequency range of operation (0.8 to 2.5 GHz). The effects of the phase slope and amplitude variations on the pattern of a linear array were determined by simulations that incorporated the measured data. The simulation showed unacceptable beam squint with frequency. Therefore, it appears that the AD8346EVAL modulator can only be used over a portion of the specified band. That is, the tunable bandwidth may be from 0.8 to 2.5 GHz, but the instantaneous bandwidth will be significantly less.

On the receive side, the AD8347EVAL demodulator board was successfully configured to operate as a phase shifter. Phase shifted transmit signals were injected into the demodulator, and corresponding phase shifts were measured via the *I* and *Q* voltages. A periodic phase error was identified and attributed to the phase error inherent in the modulator board.

B. RECOMMENDATIONS FOR FUTURE WORK

1. Arrays Transmit Antenna with Time Delay Unit

The next step in the transmit antenna research is to determine if some type of time delay unit can be applied so as to increase the instantaneous bandwidth of the modulator board. The time delay unit can be implemented either analog RF TDU or digital time delay filter.

Analog RF TDU is large, expensive, and is likely to introduce quantization error and band edge phase error [9]. On the other hand, a digital time delay filter may consist of an ADC, a digital delay filter, and DAC [10]. All these components are small and it is

more adaptable to the changing phase that is required in each element since it is usually implemented in software. However, software TDUs are difficult to implement on the transmit antenna. The waveform into the modulator would have to be modified so that the waveform spectrum multiplied by the frequency characteristic of the modulator gives the desired broadband performance.

2. Transmit Antenna with Amplitude Equalizers

The measured frequency-magnitude response plot of the AD8346EVAL board (Figures 17) showed that the magnitude is not constant. Therefore, some equalization process is required to obtain constant magnitude across all of the operating frequencies.

3. Receive Antenna

The next step in the receive antenna research is to integrate the AD8347EVAL board with a compatible ADC. The ADC could then connect to a computer with digital processing capability to form the receive beams.

A 3-D phased array receive antenna could then be built with the necessary I/O boards to allow the GA to be verified for the entire beam forming process from transmission to reception as shown in Figure 28.

APPENDIX A: GLOSSARY OF TERMINOLOGY

3-D	Three Dimensional
AD	Analog Devices
ADC	Analog-to-Digital-Converter
AF	Array Factor
AGC	Auto Gain Control
CDMA	Code Division Multiple Access
COTS	Commercial Off The Shelf
GA	Genetic Algorithm
GHz	Giga Hertz
GSM	Global Satellite Mobile
I/O	Input/Output
IR	Infrared
LCDR	Lieutenant Commander
LO	Local Oscillator
NI	National Instruments
RCS	Radar Cross Section
RF	Radio Frequency
RFIC	Radio Frequency Integrated Circuit
TDSI	Temasek Defense Systems Institute
TDU	Time Delay Unit
UHF/VHF	Ultra High Frequency/Very High Frequency
VNA	Vector Network Analyzer

THIS PAGE INTENTIONALLY LEFT BLANK

APPENDIX B: MATLAB CODE OF THE PHASED ARRAY TRANSMIT ANTENNA FOR GENERATING FIGURES 17 TO 20

```
%Analysis of the measured data for the phased array transmit antenna.
%The S21 parameters are loaded to calculate the amplitudes and phases of the AD8346EVAL board.
%The amplitudes and phases versus frequency response are plotted in Figure 17 to 20.


clear
load Test_0.m, load Test_15.m, load Test_30.m, load Test_45.m, load Test_60.m;
load Test_75.m, load Test_90.m, load Test_105.m, load Test_120.m, load Test_135.m;
load Test_150.m, load Test_165.m, load Test_180.m, load Test_195.m, load Test_210.m;
load Test_225.m, load Test_240.m, load Test_255.m, load Test_270.m, load Test_285.m;
load Test_300.m, load Test_315.m, load Test_330.m, load Test_345.m,

%Frequency sweep from 0.8 to 2.5 GHz with 201 samplers.
fstart = 0.8;
fstop = 2.5;
nf = 201;
fstep = (fstop - fstart)/(nf -1);
f = [fstart:fstep:fstop];

%Convert the data to real and imaginery parts.
I0 = Test_0(:,1);
Q0 = Test_0(:,2);
V0 = I0 + j*Q0;

I15 = Test_15(:,1);
Q15 = Test_15(:,2);
V15 = I15 + j*Q15;

I30 = Test_30(:,1);
Q30 = Test_30(:,2);
V30 = I30 + j*Q30;

I45 = Test_45(:,1);
Q45 = Test_45(:,2);
V45 = I45 + j*Q45;

I60 = Test_60(:,1);
Q60 = Test_60(:,2);
V60 = I60 + j*Q60;

I75 = Test_75(:,1);
Q75 = Test_75(:,2);
V75 = I75 + j*Q75;

I90 = Test_90(:,1);
Q90 = Test_90(:,2);
V90 = I90 + j*Q90;

I105 = Test_105(:,1);
Q105 = Test_105(:,2);
V105 = I105 + j*Q105;

I120 = Test_120(:,1);
Q120 = Test_120(:,2);
V120 = I120 + j*Q120;
```

```
I135 = Test_135(:,1);
Q135 = Test_135(:,2);
V135 = I135 + j*Q135;

I150 = Test_150(:,1);
Q150 = Test_150(:,2);
V150 = I150 + j*Q150;

I165 = Test_165(:,1);
Q165 = Test_165(:,2);
V165 = I165 + j*Q165;

I180 = Test_180(:,1);
Q180 = Test_180(:,2);
V180 = I180 + j*Q180;

I195 = Test_195(:,1);
Q195 = Test_195(:,2);
V195 = I195 + j*Q195;

I210 = Test_210(:,1);
Q210 = Test_210(:,2);
V210 = I210 + j*Q210;

I225 = Test_225(:,1);
Q225 = Test_225(:,2);
V225 = I225 + j*Q225;

I240 = Test_240(:,1);
Q240 = Test_240(:,2);
V240 = I240 + j*Q240;

I255 = Test_255(:,1);
Q255 = Test_255(:,2);
V255 = I255 + j*Q255;

I270 = Test_270(:,1);
Q270 = Test_270(:,2);
V270 = I270 + j*Q270;

I285 = Test_285(:,1);
Q285 = Test_285(:,2);
V285 = I285 + j*Q285;

I300 = Test_300(:,1);
Q300 = Test_300(:,2);
V300 = I300 + j*Q300;

I315 = Test_315(:,1);
Q315 = Test_315(:,2);
V315 = I315 + j*Q315;

I330 = Test_330(:,1);
Q330 = Test_330(:,2);
V330 = I330 + j*Q330;

I345 = Test_345(:,1);
Q345 = Test_345(:,2);
V345 = I345 + j*Q345;

%Convert to magnitude and phase.
Mag0 = 10*log(abs(V0)), Phase0 = unwrap(angle(V0))*(180/pi);
```

```
Mag15 = 10*log(abs(V15)), Phase15 = unwrap(angle(V15))*(180/pi);
Mag30 = 10*log(abs(V30)), Phase30 = unwrap(angle(V30))*(180/pi);
Mag45 = 10*log(abs(V45)), Phase45 = unwrap(angle(V45))*(180/pi);
Mag60 = 10*log(abs(V60)), Phase60 = unwrap(angle(V60))*(180/pi);
Mag75 = 10*log(abs(V75)), Phase75 = unwrap(angle(V75))*(180/pi);
Mag90 = 10*log(abs(V90)), Phase90 = unwrap(angle(V90))*(180/pi);
Mag105 = 10*log(abs(V105)), Phase105 = unwrap(angle(V105))*(180/pi);
Mag120 = 10*log(abs(V120)), Phase120 = unwrap(angle(V120))*(180/pi);
Mag135 = 10*log(abs(V135)), Phase135 = unwrap(angle(V135))*(180/pi);
Mag150 = 10*log(abs(V150)), Phase150 = unwrap(angle(V150))*(180/pi);
Mag165 = 10*log(abs(V165)), Phase165 = unwrap(angle(V165))*(180/pi);
Mag180 = 10*log(abs(V180)), Phase180 = unwrap(angle(V180))*(180/pi);
Mag195 = 10*log(abs(V195)),Phase195 = unwrap(angle(V195))*(180/pi);
Mag210 = 10*log(abs(V210)), Phase210 = unwrap(angle(V210))*(180/pi);
Mag225 = 10*log(abs(V225)), Phase225 = unwrap(angle(V225))*(180/pi);
Mag240 = 10*log(abs(V240)), Phase240 = unwrap(angle(V240))*(180/pi);
Mag255 = 10*log(abs(V255)), Phase255 = unwrap(angle(V255))*(180/pi);
Mag270 = 10*log(abs(V270)), Phase270 = unwrap(angle(V270))*(180/pi);
Mag285 = 10*log(abs(V285)), Phase285 = unwrap(angle(V285))*(180/pi);
Mag300 = 10*log(abs(V300)), Phase300 = unwrap(angle(V300))*(180/pi);
Mag315 = 10*log(abs(V315)), Phase315 = unwrap(angle(V315))*(180/pi);
Mag330 = 10*log(abs(V330)), Phase330 = unwrap(angle(V330))*(180/pi);
Mag345 = 10*log(abs(V345)), Phase345 = unwrap(angle(V345))*(180/pi);

subplot(211)
%figure(1)
plot(f,Mag0,f,Mag15,f,Mag30,f,Mag45,f,Mag60,f,Mag75)
legend('0 degree','15 degrees','30 degrees','45 degrees','60 degrees','75 degrees');
xlabel('Frequency (GHz)');
ylabel('Magnitude (dB)');
title('Frequency-Magnitude Response');
%print -depsc -tiff -r300 magnitude1

subplot(212)
%figure(2)
plot(f,Phase0,f,Phase15,f,Phase30,f,Phase45,f,Phase60,f,Phase75)
legend('0 degree','15 degrees','30 degrees','45 degrees','60 degrees','75 degrees');
xlabel('Frequency (GHz)')
ylabel('Phase (degrees)')
title('Frequency-Phase Response')
print -depsc -tiff -r300 mag_phase1
```

THIS PAGE INTENTIONALLY LEFT BLANK

APPENDIX C: MATHCAD CODE FOR SIMULATING THE RADIATION PATTERN OF THE LINEAR PHASED ARRAY

We will assume a N-element linear array with uniformly-spaced identical elements. We will assume that all is happening in the xz-plane.

$X := 201$

$Y := 2$

$x := 0 .. X - 1$

$y := 0 .. Y - 1$

$j := \sqrt{-1}$

Frequency Range: 0.8 - 2.5 GHz with 201 data points.

$f_{start} := 0.8$

$f_{stop} := 2.5$

$$\Delta f := \frac{\left(f_{stop} - f_{start}\right)}{X - 1}$$

$\Delta f = 8.5 \times 10^{-3}$

$freq_x := x \cdot \Delta f + f_{start}$

Reading Transmitter's data files. Total 360 files at 1 degree increment

Deg0:= READPRN("Test_0.txt")
Deg1:= READPRN("Test_1.txt")
.
.
.
.
.
.
Deg358:= READPRN("Test_358.txt")
Deg359:= READPRN("Test_359.txt")

Defining the vectors. Converting to real and imaginary parts for 360 measured data.

$Vector\_0_x := Deg0_{x,0} + j \cdot Deg0_{x,1}$

$Vector\_1_x := Deg1_{x,0} + j \cdot Deg1_{x,1}$

$Vector\_2_x := Deg2_{x,0} + j \cdot Deg2_{x,1}$

$Vector\_3_x := Deg3_{x,0} + j \cdot Deg3_{x,1}$

$Vector\_4_x := Deg4_{x,0} + j \cdot Deg4_{x,1}$

$Vector\_5_x := Deg5_{x,0} + j \cdot Deg5_{x,1}$

$Vector\_6_x := Deg6_{x,0} + j \cdot Deg6_{x,1}$

$Vector\_7_x := Deg7_{x,0} + j \cdot Deg7_{x,1}$

$Vector\_8_x := Deg8_{x,0} + j \cdot Deg8_{x,1}$

$Vector\_9_x := Deg9_{x,0} + j \cdot Deg9_{x,1}$

$Vector\_10_x := Deg10_{x,0} + j \cdot Deg10_{x,1}$

$Vector\_11_x := Deg11_{x,0} + j \cdot Deg11_{x,1}$

$Vector\_181_x := Deg181_{x,0} + j \cdot Deg181_{x,1}$

$Vector\_182_x := Deg182_{x,0} + j \cdot Deg182_{x,1}$

$Vector\_183_x := Deg183_{x,0} + j \cdot Deg183_{x,1}$

$Vector\_184_x := Deg184_{x,0} + j \cdot Deg184_{x,1}$

$Vector\_185_x := Deg185_{x,0} + j \cdot Deg185_{x,1}$

$Vector\_186_x := Deg186_{x,0} + j \cdot Deg186_{x,1}$

$Vector\_187_x := Deg187_{x,0} + j \cdot Deg187_{x,1}$

$Vector\_188_x := Deg188_{x,0} + j \cdot Deg188_{x,1}$

$Vector\_189_x := Deg189_{x,0} + j \cdot Deg189_{x,1}$

$Vector\_190_x := Deg190_{x,0} + j \cdot Deg190_{x,1}$

$Vector\_191_x := Deg191_{x,0} + j \cdot Deg191_{x,1}$

$Vector\_192_x := Deg192_{x,0} + j \cdot Deg192_{x,1}$

$Vector\_12_x := Deg12_{x,0} + j \cdot Deg12_{x,1}$

$Vector\_13_x := Deg13_{x,0} + j \cdot Deg13_{x,1}$

$Vector\_14_x := Deg14_{x,0} + j \cdot Deg14_{x,1}$

$Vector\_15_x := Deg15_{x,0} + j \cdot Deg15_{x,1}$

$Vector\_16_x := Deg16_{x,0} + j \cdot Deg16_{x,1}$

$Vector\_17_x := Deg17_{x,0} + j \cdot Deg17_{x,1}$

$Vector\_18_x := Deg18_{x,0} + j \cdot Deg18_{x,1}$

$Vector\_19_x := Deg19_{x,0} + j \cdot Deg19_{x,1}$

$Vector\_20_x := Deg20_{x,0} + j \cdot Deg20_{x,1}$

$Vector\_21_x := Deg21_{x,0} + j \cdot Deg21_{x,1}$

$Vector\_22_x := Deg22_{x,0} + j \cdot Deg22_{x,1}$

$Vector\_23_x := Deg23_{x,0} + j \cdot Deg23_{x,1}$

$Vector\_24_x := Deg24_{x,0} + j \cdot Deg24_{x,1}$

$Vector\_25_x := Deg25_{x,0} + j \cdot Deg25_{x,1}$

$Vector\_26_x := Deg26_{x,0} + j \cdot Deg26_{x,1}$

$Vector\_27_x := Deg27_{x,0} + j \cdot Deg27_{x,1}$

$Vector\_28_x := Deg28_{x,0} + j \cdot Deg28_{x,1}$

$Vector\_29_x := Deg29_{x,0} + j \cdot Deg29_{x,1}$

$Vector\_30_x := Deg30_{x,0} + j \cdot Deg30_{x,1}$

$Vector\_31_x := Deg31_{x,0} + j \cdot Deg31_{x,1}$

$Vector\_32_x := Deg32_{x,0} + j \cdot Deg32_{x,1}$

$Vector\_33_x := Deg33_{x,0} + j \cdot Deg33_{x,1}$

$Vector\_34_x := Deg34_{x,0} + j \cdot Deg34_{x,1}$

$Vector\_35_x := Deg35_{x,0} + j \cdot Deg35_{x,1}$

$Vector\_36_x := Deg36_{x,0} + j \cdot Deg36_{x,1}$

$Vector\_37_x := Deg37_{x,0} + j \cdot Deg37_{x,1}$

$Vector\_38_x := Deg38_{x,0} + j \cdot Deg38_{x,1}$

$Vector\_39_x := Deg39_{x,0} + j \cdot Deg39_{x,1}$

$Vector\_40_x := Deg40_{x,0} + j \cdot Deg40_{x,1}$

$Vector\_41_x := Deg41_{x,0} + j \cdot Deg41_{x,1}$

$Vector\_42_x := Deg42_{x,0} + j \cdot Deg42_{x,1}$

$Vector\_43_x := Deg43_{x,0} + j \cdot Deg43_{x,1}$

$Vector\_44_x := Deg44_{x,0} + j \cdot Deg44_{x,1}$

$Vector\_45_x := Deg45_{x,0} + j \cdot Deg45_{x,1}$

$Vector\_46_x := Deg46_{x,0} + j \cdot Deg46_{x,1}$

$Vector\_47_x := Deg47_{x,0} + j \cdot Deg47_{x,1}$

$Vector\_193_x := Deg193_{x,0} + j \cdot Deg193_{x,1}$

$Vector\_194_x := Deg194_{x,0} + j \cdot Deg194_{x,1}$

$Vector\_195_x := Deg195_{x,0} + j \cdot Deg195_{x,1}$

$Vector\_196_x := Deg196_{x,0} + j \cdot Deg196_{x,1}$

$Vector\_197_x := Deg197_{x,0} + j \cdot Deg197_{x,1}$

$Vector\_198_x := Deg198_{x,0} + j \cdot Deg198_{x,1}$

$Vector\_199_x := Deg199_{x,0} + j \cdot Deg199_{x,1}$

$Vector\_200_x := Deg200_{x,0} + j \cdot Deg200_{x,1}$

$Vector\_201_x := Deg201_{x,0} + j \cdot Deg201_{x,1}$

$Vector\_202_x := Deg202_{x,0} + j \cdot Deg202_{x,1}$

$Vector\_203_x := Deg203_{x,0} + j \cdot Deg203_{x,1}$

$Vector\_204_x := Deg204_{x,0} + j \cdot Deg204_{x,1}$

$Vector\_205_x := Deg205_{x,0} + j \cdot Deg205_{x,1}$

$Vector\_206_x := Deg206_{x,0} + j \cdot Deg206_{x,1}$

$Vector\_207_x := Deg207_{x,0} + j \cdot Deg207_{x,1}$

$Vector\_208_x := Deg208_{x,0} + j \cdot Deg208_{x,1}$

$Vector\_209_x := Deg209_{x,0} + j \cdot Deg209_{x,1}$

$Vector\_210_x := Deg210_{x,0} + j \cdot Deg210_{x,1}$

$Vector\_211_x := Deg211_{x,0} + j \cdot Deg211_{x,1}$

$Vector\_212_x := Deg212_{x,0} + j \cdot Deg212_{x,1}$

$Vector\_213_x := Deg213_{x,0} + j \cdot Deg213_{x,1}$

$Vector\_214_x := Deg214_{x,0} + j \cdot Deg214_{x,1}$

$Vector\_215_x := Deg215_{x,0} + j \cdot Deg215_{x,1}$

$Vector\_216_x := Deg216_{x,0} + j \cdot Deg216_{x,1}$

$Vector\_217_x := Deg217_{x,0} + j \cdot Deg217_{x,1}$

$Vector\_218_x := Deg218_{x,0} + j \cdot Deg218_{x,1}$

$Vector\_219_x := Deg219_{x,0} + j \cdot Deg219_{x,1}$

$Vector\_220_x := Deg220_{x,0} + j \cdot Deg220_{x,1}$

$Vector\_221_x := Deg221_{x,0} + j \cdot Deg221_{x,1}$

$Vector\_222_x := Deg222_{x,0} + j \cdot Deg222_{x,1}$

$Vector\_223_x := Deg223_{x,0} + j \cdot Deg223_{x,1}$

$Vector\_224_x := Deg224_{x,0} + j \cdot Deg224_{x,1}$

$Vector\_225_x := Deg225_{x,0} + j \cdot Deg225_{x,1}$

$Vector\_226_x := Deg226_{x,0} + j \cdot Deg226_{x,1}$

$Vector\_227_x := Deg227_{x,0} + j \cdot Deg227_{x,1}$

$Vector\_228_x := Deg228_{x,0} + j \cdot Deg228_{x,1}$

$Vector\_48_x := Deg48_{x,0} + j \cdot Deg48_{x,1}$

$Vector\_49_x := Deg49_{x,0} + j \cdot Deg49_{x,1}$

$Vector\_50_x := Deg50_{x,0} + j \cdot Deg50_{x,1}$

$Vector\_51_x := Deg51_{x,0} + j \cdot Deg51_{x,1}$

$Vector\_52_x := Deg52_{x,0} + j \cdot Deg52_{x,1}$

$Vector\_53_x := Deg53_{x,0} + j \cdot Deg53_{x,1}$

$Vector\_54_x := Deg54_{x,0} + j \cdot Deg54_{x,1}$

$Vector\_55_x := Deg55_{x,0} + j \cdot Deg55_{x,1}$

$Vector\_56_x := Deg56_{x,0} + j \cdot Deg56_{x,1}$

$Vector\_57_x := Deg57_{x,0} + j \cdot Deg57_{x,1}$

$Vector\_58_x := Deg58_{x,0} + j \cdot Deg58_{x,1}$

$Vector\_59_x := Deg59_{x,0} + j \cdot Deg59_{x,1}$

$Vector\_60_x := Deg60_{x,0} + j \cdot Deg60_{x,1}$

$Vector\_61_x := Deg61_{x,0} + j \cdot Deg61_{x,1}$

$Vector\_62_x := Deg62_{x,0} + j \cdot Deg62_{x,1}$

$Vector\_63_x := Deg63_{x,0} + j \cdot Deg63_{x,1}$

$Vector\_64_x := Deg64_{x,0} + j \cdot Deg64_{x,1}$

$Vector\_65_x := Deg65_{x,0} + j \cdot Deg65_{x,1}$

$Vector\_66_x := Deg66_{x,0} + j \cdot Deg66_{x,1}$

$Vector\_67_x := Deg67_{x,0} + j \cdot Deg67_{x,1}$

$Vector\_68_x := Deg68_{x,0} + j \cdot Deg68_{x,1}$

$Vector\_69_x := Deg69_{x,0} + j \cdot Deg69_{x,1}$

$Vector\_70_x := Deg70_{x,0} + j \cdot Deg70_{x,1}$

$Vector\_71_x := Deg71_{x,0} + j \cdot Deg71_{x,1}$

$Vector\_72_x := Deg72_{x,0} + j \cdot Deg72_{x,1}$

$Vector\_73_x := Deg73_{x,0} + j \cdot Deg73_{x,1}$

$Vector\_74_x := Deg74_{x,0} + j \cdot Deg74_{x,1}$

$Vector\_75_x := Deg75_{x,0} + j \cdot Deg75_{x,1}$

$Vector\_76_x := Deg76_{x,0} + j \cdot Deg76_{x,1}$

$Vector\_77_x := Deg77_{x,0} + j \cdot Deg77_{x,1}$

$Vector\_78_x := Deg78_{x,0} + j \cdot Deg78_{x,1}$

$Vector\_79_x := Deg79_{x,0} + j \cdot Deg79_{x,1}$

$Vector\_80_x := Deg80_{x,0} + j \cdot Deg80_{x,1}$

$Vector\_81_x := Deg81_{x,0} + j \cdot Deg81_{x,1}$

$Vector\_82_x := Deg82_{x,0} + j \cdot Deg82_{x,1}$

$Vector\_83_x := Deg83_{x,0} + j \cdot Deg83_{x,1}$

$Vector\_229_x := Deg229_{x,0} + j \cdot Deg229_{x,1}$

$Vector\_230_x := Deg230_{x,0} + j \cdot Deg230_{x,1}$

$Vector\_231_x := Deg231_{x,0} + j \cdot Deg231_{x,1}$

$Vector\_232_x := Deg232_{x,0} + j \cdot Deg232_{x,1}$

$Vector\_233_x := Deg233_{x,0} + j \cdot Deg233_{x,1}$

$Vector\_234_x := Deg234_{x,0} + j \cdot Deg234_{x,1}$

$Vector\_235_x := Deg235_{x,0} + j \cdot Deg235_{x,1}$

$Vector\_236_x := Deg236_{x,0} + j \cdot Deg236_{x,1}$

$Vector\_237_x := Deg237_{x,0} + j \cdot Deg237_{x,1}$

$Vector\_238_x := Deg238_{x,0} + j \cdot Deg238_{x,1}$

$Vector\_239_x := Deg239_{x,0} + j \cdot Deg239_{x,1}$

$Vector\_240_x := Deg240_{x,0} + j \cdot Deg240_{x,1}$

$Vector\_241_x := Deg241_{x,0} + j \cdot Deg241_{x,1}$

$Vector\_242_x := Deg242_{x,0} + j \cdot Deg242_{x,1}$

$Vector\_243_x := Deg243_{x,0} + j \cdot Deg243_{x,1}$

$Vector\_244_x := Deg244_{x,0} + j \cdot Deg244_{x,1}$

$Vector\_245_x := Deg245_{x,0} + j \cdot Deg245_{x,1}$

$Vector\_246_x := Deg246_{x,0} + j \cdot Deg246_{x,1}$

$Vector\_247_x := Deg247_{x,0} + j \cdot Deg247_{x,1}$

$Vector\_248_x := Deg248_{x,0} + j \cdot Deg248_{x,1}$

$Vector\_249_x := Deg249_{x,0} + j \cdot Deg249_{x,1}$

$Vector\_250_x := Deg250_{x,0} + j \cdot Deg250_{x,1}$

$Vector\_251_x := Deg251_{x,0} + j \cdot Deg251_{x,1}$

$Vector\_252_x := Deg252_{x,0} + j \cdot Deg252_{x,1}$

$Vector\_253_x := Deg253_{x,0} + j \cdot Deg253_{x,1}$

$Vector\_254_x := Deg254_{x,0} + j \cdot Deg254_{x,1}$

$Vector\_255_x := Deg255_{x,0} + j \cdot Deg255_{x,1}$

$Vector\_256_x := Deg256_{x,0} + j \cdot Deg256_{x,1}$

$Vector\_257_x := Deg257_{x,0} + j \cdot Deg257_{x,1}$

$Vector\_258_x := Deg258_{x,0} + j \cdot Deg258_{x,1}$

$Vector\_259_x := Deg259_{x,0} + j \cdot Deg259_{x,1}$

$Vector\_260_x := Deg260_{x,0} + j \cdot Deg260_{x,1}$

$Vector\_261_x := Deg261_{x,0} + j \cdot Deg261_{x,1}$

$Vector\_262_x := Deg262_{x,0} + j \cdot Deg262_{x,1}$

$Vector\_263_x := Deg263_{x,0} + j \cdot Deg263_{x,1}$

$Vector\_264_x := Deg264_{x,0} + j \cdot Deg264_{x,1}$

$Vector\_84_x := Deg84_{x,0} + j \cdot Deg84_{x,1}$

$Vector\_85_x := Deg85_{x,0} + j \cdot Deg85_{x,1}$

$Vector\_86_x := Deg86_{x,0} + j \cdot Deg86_{x,1}$

$Vector\_87_x := Deg87_{x,0} + j \cdot Deg87_{x,1}$

$Vector\_88_x := Deg88_{x,0} + j \cdot Deg88_{x,1}$

$Vector\_89_x := Deg89_{x,0} + j \cdot Deg89_{x,1}$

$Vector\_90_x := Deg90_{x,0} + j \cdot Deg90_{x,1}$

$Vector\_91_x := Deg91_{x,0} + j \cdot Deg91_{x,1}$

$Vector\_92_x := Deg92_{x,0} + j \cdot Deg92_{x,1}$

$Vector\_93_x := Deg93_{x,0} + j \cdot Deg93_{x,1}$

$Vector\_94_x := Deg94_{x,0} + j \cdot Deg94_{x,1}$

$Vector\_95_x := Deg95_{x,0} + j \cdot Deg95_{x,1}$

$Vector\_96_x := Deg96_{x,0} + j \cdot Deg96_{x,1}$

$Vector\_97_x := Deg97_{x,0} + j \cdot Deg97_{x,1}$

$Vector\_98_x := Deg98_{x,0} + j \cdot Deg98_{x,1}$

$Vector\_99_x := Deg99_{x,0} + j \cdot Deg99_{x,1}$

$Vector\_100_x := Deg100_{x,0} + j \cdot Deg100_{x,1}$

$Vector\_101_x := Deg101_{x,0} + j \cdot Deg101_{x,1}$

$Vector\_102_x := Deg102_{x,0} + j \cdot Deg102_{x,1}$

$Vector\_103_x := Deg103_{x,0} + j \cdot Deg103_{x,1}$

$Vector\_104_x := Deg104_{x,0} + j \cdot Deg104_{x,1}$

$Vector\_105_x := Deg105_{x,0} + j \cdot Deg105_{x,1}$

$Vector\_106_x := Deg106_{x,0} + j \cdot Deg106_{x,1}$

$Vector\_107_x := Deg107_{x,0} + j \cdot Deg107_{x,1}$

$Vector\_108_x := Deg108_{x,0} + j \cdot Deg108_{x,1}$

$Vector\_109_x := Deg109_{x,0} + j \cdot Deg109_{x,1}$

$Vector\_110_x := Deg110_{x,0} + j \cdot Deg110_{x,1}$

$Vector\_111_x := Deg111_{x,0} + j \cdot Deg111_{x,1}$

$Vector\_112_x := Deg112_{x,0} + j \cdot Deg112_{x,1}$

$Vector\_113_x := Deg113_{x,0} + j \cdot Deg113_{x,1}$

$Vector\_114_x := Deg114_{x,0} + j \cdot Deg114_{x,1}$

$Vector\_115_x := Deg115_{x,0} + j \cdot Deg115_{x,1}$

$Vector\_116_x := Deg116_{x,0} + j \cdot Deg116_{x,1}$

$Vector\_117_x := Deg117_{x,0} + j \cdot Deg117_{x,1}$

$Vector\_118_x := Deg118_{x,0} + j \cdot Deg118_{x,1}$

$Vector\_119_x := Deg119_{x,0} + j \cdot Deg119_{x,1}$

$Vector\_265_x := Deg265_{x,0} + j \cdot Deg265_{x,1}$

$Vector\_266_x := Deg266_{x,0} + j \cdot Deg266_{x,1}$

$Vector\_267_x := Deg267_{x,0} + j \cdot Deg267_{x,1}$

$Vector\_268_x := Deg268_{x,0} + j \cdot Deg268_{x,1}$

$Vector\_269_x := Deg269_{x,0} + j \cdot Deg269_{x,1}$

$Vector\_270_x := Deg270_{x,0} + j \cdot Deg270_{x,1}$

$Vector\_271_x := Deg271_{x,0} + j \cdot Deg271_{x,1}$

$Vector\_272_x := Deg272_{x,0} + j \cdot Deg272_{x,1}$

$Vector\_273_x := Deg273_{x,0} + j \cdot Deg273_{x,1}$

$Vector\_274_x := Deg274_{x,0} + j \cdot Deg274_{x,1}$

$Vector\_275_x := Deg275_{x,0} + j \cdot Deg275_{x,1}$

$Vector\_276_x := Deg276_{x,0} + j \cdot Deg276_{x,1}$

$Vector\_277_x := Deg277_{x,0} + j \cdot Deg277_{x,1}$

$Vector\_278_x := Deg278_{x,0} + j \cdot Deg278_{x,1}$

$Vector\_279_x := Deg279_{x,0} + j \cdot Deg279_{x,1}$

$Vector\_280_x := Deg280_{x,0} + j \cdot Deg280_{x,1}$

$Vector\_281_x := Deg281_{x,0} + j \cdot Deg281_{x,1}$

$Vector\_282_x := Deg282_{x,0} + j \cdot Deg282_{x,1}$

$Vector\_283_x := Deg283_{x,0} + j \cdot Deg283_{x,1}$

$Vector\_284_x := Deg284_{x,0} + j \cdot Deg284_{x,1}$

$Vector\_285_x := Deg285_{x,0} + j \cdot Deg285_{x,1}$

$Vector\_286_x := Deg286_{x,0} + j \cdot Deg286_{x,1}$

$Vector\_287_x := Deg287_{x,0} + j \cdot Deg287_{x,1}$

$Vector\_288_x := Deg288_{x,0} + j \cdot Deg288_{x,1}$

$Vector\_289_x := Deg289_{x,0} + j \cdot Deg289_{x,1}$

$Vector\_290_x := Deg290_{x,0} + j \cdot Deg290_{x,1}$

$Vector\_291_x := Deg291_{x,0} + j \cdot Deg291_{x,1}$

$Vector\_292_x := Deg292_{x,0} + j \cdot Deg292_{x,1}$

$Vector\_293_x := Deg293_{x,0} + j \cdot Deg293_{x,1}$

$Vector\_294_x := Deg294_{x,0} + j \cdot Deg294_{x,1}$

$Vector\_295_x := Deg295_{x,0} + j \cdot Deg295_{x,1}$

$Vector\_296_x := Deg296_{x,0} + j \cdot Deg296_{x,1}$

$Vector\_297_x := Deg297_{x,0} + j \cdot Deg297_{x,1}$

$Vector\_298_x := Deg298_{x,0} + j \cdot Deg298_{x,1}$

$Vector\_299_x := Deg299_{x,0} + j \cdot Deg299_{x,1}$

$Vector\_300_x := Deg300_{x,0} + j \cdot Deg300_{x,1}$

$Vector\_120_x := Deg120_{x,0} + j \cdot Deg120_{x,1}$

$Vector\_121_x := Deg121_{x,0} + j \cdot Deg121_{x,1}$

$Vector\_122_x := Deg122_{x,0} + j \cdot Deg122_{x,1}$

$Vector\_123_x := Deg123_{x,0} + j \cdot Deg123_{x,1}$

$Vector\_124_x := Deg124_{x,0} + j \cdot Deg124_{x,1}$

$Vector\_125_x := Deg125_{x,0} + j \cdot Deg125_{x,1}$

$Vector\_126_x := Deg126_{x,0} + j \cdot Deg126_{x,1}$

$Vector\_127_x := Deg127_{x,0} + j \cdot Deg127_{x,1}$

$Vector\_128_x := Deg128_{x,0} + j \cdot Deg128_{x,1}$

$Vector\_129_x := Deg129_{x,0} + j \cdot Deg129_{x,1}$

$Vector\_130_x := Deg130_{x,0} + j \cdot Deg130_{x,1}$

$Vector\_131_x := Deg131_{x,0} + j \cdot Deg131_{x,1}$

$Vector\_132_x := Deg132_{x,0} + j \cdot Deg132_{x,1}$

$Vector\_133_x := Deg133_{x,0} + j \cdot Deg133_{x,1}$

$Vector\_134_x := Deg134_{x,0} + j \cdot Deg134_{x,1}$

$Vector\_135_x := Deg135_{x,0} + j \cdot Deg135_{x,1}$

$Vector\_136_x := Deg136_{x,0} + j \cdot Deg136_{x,1}$

$Vector\_137_x := Deg137_{x,0} + j \cdot Deg137_{x,1}$

$Vector\_138_x := Deg138_{x,0} + j \cdot Deg138_{x,1}$

$Vector\_139_x := Deg139_{x,0} + j \cdot Deg139_{x,1}$

$Vector\_140_x := Deg140_{x,0} + j \cdot Deg140_{x,1}$

$Vector\_141_x := Deg141_{x,0} + j \cdot Deg141_{x,1}$

$Vector\_142_x := Deg142_{x,0} + j \cdot Deg142_{x,1}$

$Vector\_143_x := Deg143_{x,0} + j \cdot Deg143_{x,1}$

$Vector\_144_x := Deg144_{x,0} + j \cdot Deg144_{x,1}$

$Vector\_145_x := Deg145_{x,0} + j \cdot Deg145_{x,1}$

$Vector\_146_x := Deg146_{x,0} + j \cdot Deg146_{x,1}$

$Vector\_147_x := Deg147_{x,0} + j \cdot Deg147_{x,1}$

$Vector\_148_x := Deg148_{x,0} + j \cdot Deg148_{x,1}$

$Vector\_149_x := Deg149_{x,0} + j \cdot Deg149_{x,1}$

$Vector\_150_x := Deg150_{x,0} + j \cdot Deg150_{x,1}$

$Vector\_151_x := Deg151_{x,0} + j \cdot Deg151_{x,1}$

$Vector\_152_x := Deg152_{x,0} + j \cdot Deg152_{x,1}$

$Vector\_153_x := Deg153_{x,0} + j \cdot Deg153_{x,1}$

$Vector\_154_x := Deg154_{x,0} + j \cdot Deg154_{x,1}$

$Vector\_155_x := Deg155_{x,0} + j \cdot Deg155_{x,1}$

$Vector\_301_x := Deg301_{x,0} + j \cdot Deg301_{x,1}$

$Vector\_302_x := Deg302_{x,0} + j \cdot Deg302_{x,1}$

$Vector\_303_x := Deg303_{x,0} + j \cdot Deg303_{x,1}$

$Vector\_304_x := Deg304_{x,0} + j \cdot Deg304_{x,1}$

$Vector\_305_x := Deg305_{x,0} + j \cdot Deg305_{x,1}$

$Vector\_306_x := Deg306_{x,0} + j \cdot Deg306_{x,1}$

$Vector\_307_x := Deg307_{x,0} + j \cdot Deg307_{x,1}$

$Vector\_308_x := Deg308_{x,0} + j \cdot Deg308_{x,1}$

$Vector\_309_x := Deg309_{x,0} + j \cdot Deg309_{x,1}$

$Vector\_310_x := Deg310_{x,0} + j \cdot Deg310_{x,1}$

$Vector\_311_x := Deg311_{x,0} + j \cdot Deg311_{x,1}$

$Vector\_312_x := Deg312_{x,0} + j \cdot Deg312_{x,1}$

$Vector\_313_x := Deg313_{x,0} + j \cdot Deg313_{x,1}$

$Vector\_314_x := Deg314_{x,0} + j \cdot Deg314_{x,1}$

$Vector\_315_x := Deg315_{x,0} + j \cdot Deg315_{x,1}$

$Vector\_316_x := Deg316_{x,0} + j \cdot Deg316_{x,1}$

$Vector\_317_x := Deg317_{x,0} + j \cdot Deg317_{x,1}$

$Vector\_318_x := Deg318_{x,0} + j \cdot Deg318_{x,1}$

$Vector\_319_x := Deg319_{x,0} + j \cdot Deg319_{x,1}$

$Vector\_320_x := Deg320_{x,0} + j \cdot Deg320_{x,1}$

$Vector\_321_x := Deg321_{x,0} + j \cdot Deg321_{x,1}$

$Vector\_322_x := Deg322_{x,0} + j \cdot Deg322_{x,1}$

$Vector\_323_x := Deg323_{x,0} + j \cdot Deg323_{x,1}$

$Vector\_324_x := Deg324_{x,0} + j \cdot Deg324_{x,1}$

$Vector\_325_x := Deg325_{x,0} + j \cdot Deg325_{x,1}$

$Vector\_326_x := Deg326_{x,0} + j \cdot Deg326_{x,1}$

$Vector\_327_x := Deg327_{x,0} + j \cdot Deg327_{x,1}$

$Vector\_328_x := Deg328_{x,0} + j \cdot Deg328_{x,1}$

$Vector\_329_x := Deg329_{x,0} + j \cdot Deg329_{x,1}$

$Vector\_330_x := Deg330_{x,0} + j \cdot Deg330_{x,1}$

$Vector\_331_x := Deg331_{x,0} + j \cdot Deg331_{x,1}$

$Vector\_332_x := Deg332_{x,0} + j \cdot Deg332_{x,1}$

$Vector\_333_x := Deg333_{x,0} + j \cdot Deg333_{x,1}$

$Vector\_334_x := Deg334_{x,0} + j \cdot Deg334_{x,1}$

$Vector\_335_x := Deg335_{x,0} + j \cdot Deg335_{x,1}$

$Vector\_336_x := Deg336_{x,0} + j \cdot Deg336_{x,1}$

$Vector\_156_x := Deg156_{x,0} + j \cdot Deg156_{x,1}$
$Vector\_157_x := Deg157_{x,0} + j \cdot Deg157_{x,1}$
$Vector\_158_x := Deg158_{x,0} + j \cdot Deg158_{x,1}$
$Vector\_159_x := Deg159_{x,0} + j \cdot Deg159_{x,1}$
$Vector\_160_x := Deg160_{x,0} + j \cdot Deg160_{x,1}$
$Vector\_161_x := Deg161_{x,0} + j \cdot Deg161_{x,1}$
$Vector\_162_x := Deg162_{x,0} + j \cdot Deg162_{x,1}$
$Vector\_163_x := Deg163_{x,0} + j \cdot Deg163_{x,1}$
$Vector\_164_x := Deg164_{x,0} + j \cdot Deg164_{x,1}$
$Vector\_165_x := Deg165_{x,0} + j \cdot Deg165_{x,1}$
$Vector\_166_x := Deg166_{x,0} + j \cdot Deg166_{x,1}$
$Vector\_167_x := Deg167_{x,0} + j \cdot Deg167_{x,1}$
$Vector\_168_x := Deg168_{x,0} + j \cdot Deg168_{x,1}$
$Vector\_169_x := Deg169_{x,0} + j \cdot Deg169_{x,1}$
$Vector\_170_x := Deg170_{x,0} + j \cdot Deg170_{x,1}$
$Vector\_171_x := Deg171_{x,0} + j \cdot Deg171_{x,1}$
$Vector\_172_x := Deg172_{x,0} + j \cdot Deg172_{x,1}$
$Vector\_173_x := Deg173_{x,0} + j \cdot Deg173_{x,1}$
$Vector\_174_x := Deg174_{x,0} + j \cdot Deg174_{x,1}$
$Vector\_175_x := Deg175_{x,0} + j \cdot Deg175_{x,1}$
$Vector\_176_x := Deg176_{x,0} + j \cdot Deg176_{x,1}$
$Vector\_177_x := Deg177_{x,0} + j \cdot Deg177_{x,1}$
$Vector\_178_x := Deg178_{x,0} + j \cdot Deg178_{x,1}$
$Vector\_179_x := Deg179_{x,0} + j \cdot Deg179_{x,1}$
$Vector\_180_x := Deg180_{x,0} + j \cdot Deg180_{x,1}$

$Vector\_337_x := Deg337_{x,0} + j \cdot Deg337_{x,1}$
$Vector\_338_x := Deg338_{x,0} + j \cdot Deg338_{x,1}$
$Vector\_339_x := Deg339_{x,0} + j \cdot Deg339_{x,1}$
$Vector\_340_x := Deg340_{x,0} + j \cdot Deg340_{x,1}$
$Vector\_341_x := Deg341_{x,0} + j \cdot Deg341_{x,1}$
$Vector\_342_x := Deg342_{x,0} + j \cdot Deg342_{x,1}$
$Vector\_343_x := Deg343_{x,0} + j \cdot Deg343_{x,1}$
$Vector\_344_x := Deg344_{x,0} + j \cdot Deg344_{x,1}$
$Vector\_345_x := Deg345_{x,0} + j \cdot Deg345_{x,1}$
$Vector\_346_x := Deg346_{x,0} + j \cdot Deg346_{x,1}$
$Vector\_347_x := Deg347_{x,0} + j \cdot Deg347_{x,1}$
$Vector\_348_x := Deg348_{x,0} + j \cdot Deg348_{x,1}$
$Vector\_349_x := Deg349_{x,0} + j \cdot Deg349_{x,1}$
$Vector\_350_x := Deg350_{x,0} + j \cdot Deg350_{x,1}$
$Vector\_351_x := Deg351_{x,0} + j \cdot Deg351_{x,1}$
$Vector\_352_x := Deg352_{x,0} + j \cdot Deg352_{x,1}$
$Vector\_353_x := Deg353_{x,0} + j \cdot Deg353_{x,1}$
$Vector\_354_x := Deg354_{x,0} + j \cdot Deg354_{x,1}$
$Vector\_355_x := Deg355_{x,0} + j \cdot Deg355_{x,1}$
$Vector\_356_x := Deg356_{x,0} + j \cdot Deg356_{x,1}$
$Vector\_357_x := Deg357_{x,0} + j \cdot Deg357_{x,1}$
$Vector\_358_x := Deg358_{x,0} + j \cdot Deg358_{x,1}$
$Vector\_359_x := Deg359_{x,0} + j \cdot Deg359_{x,1}$

Phase shift and Amplitude for each element due to the transmitting angle:

$\alpha_0 := Vector\_0$
$\alpha_1 := Vector\_1$
$\alpha_2 := Vector\_2$
$\alpha_3 := Vector\_3$
$\alpha_4 := Vector\_4$
$\alpha_5 := Vector\_5$
$\alpha_6 := Vector\_6$
$\alpha_7 := Vector\_7$
$\alpha_8 := Vector\_8$

$\alpha_{101} := Vector\_101$
$\alpha_{102} := Vector\_102$
$\alpha_{103} := Vector\_103$
$\alpha_{104} := Vector\_104$
$\alpha_{105} := Vector\_105$
$\alpha_{106} := Vector\_106$
$\alpha_{107} := Vector\_107$
$\alpha_{108} := Vector\_108$
$\alpha_{109} := Vector\_109$

$\alpha_{201} := Vector\_201$
$\alpha_{202} := Vector\_202$
$\alpha_{203} := Vector\_203$
$\alpha_{204} := Vector\_204$
$\alpha_{205} := Vector\_205$
$\alpha_{206} := Vector\_206$
$\alpha_{207} := Vector\_207$
$\alpha_{208} := Vector\_208$
$\alpha_{209} := Vector\_209$

α_{9} := Vector_9
α_{10} := Vector_10
α_{11} := Vector_11
α_{12} := Vector_12
α_{13} := Vector_13
α_{14} := Vector_14
α_{15} := Vector_15
α_{16} := Vector_16
α_{17} := Vector_17
α_{18} := Vector_18
α_{19} := Vector_19
α_{20} := Vector_20
α_{21} := Vector_21
α_{22} := Vector_22
α_{23} := Vector_23
α_{24} := Vector_24
α_{25} := Vector_25
α_{26} := Vector_26
α_{27} := Vector_27
α_{28} := Vector_28
α_{29} := Vector_29
α_{30} := Vector_30
α_{31} := Vector_31
α_{32} := Vector_32
α_{33} := Vector_33
α_{34} := Vector_34
α_{35} := Vector_35
α_{36} := Vector_36
α_{37} := Vector_37
α_{38} := Vector_38
α_{39} := Vector_39
α_{40} := Vector_40
α_{41} := Vector_41
α_{42} := Vector_42
α_{43} := Vector_43
α_{44} := Vector_44
α_{45} := Vector_45
α_{46} := Vector_46
α_{47} := Vector_47
α_{48} := Vector_48
α_{49} := Vector_49
α_{110} := Vector_110
α_{111} := Vector_111
α_{112} := Vector_112
α_{113} := Vector_113
α_{114} := Vector_114
α_{115} := Vector_115
α_{116} := Vector_116
α_{117} := Vector_117
α_{118} := Vector_118
α_{119} := Vector_119
α_{120} := Vector_120
α_{121} := Vector_121
α_{122} := Vector_122
α_{123} := Vector_123
α_{124} := Vector_124
α_{125} := Vector_125
α_{126} := Vector_126
α_{127} := Vector_127
α_{128} := Vector_128
α_{129} := Vector_129
α_{130} := Vector_130
α_{131} := Vector_131
α_{132} := Vector_132
α_{133} := Vector_133
α_{134} := Vector_134
α_{135} := Vector_135
α_{136} := Vector_136
α_{137} := Vector_137
α_{138} := Vector_138
α_{139} := Vector_139
α_{140} := Vector_140
α_{141} := Vector_141
α_{142} := Vector_142
α_{143} := Vector_143
α_{144} := Vector_144
α_{145} := Vector_145
α_{146} := Vector_146
α_{147} := Vector_147
α_{148} := Vector_148
α_{149} := Vector_149
α_{150} := Vector_150
α_{210} := Vector_210
α_{211} := Vector_211
α_{212} := Vector_212
α_{213} := Vector_213
α_{214} := Vector_214
α_{215} := Vector_215
α_{216} := Vector_216
α_{217} := Vector_217
α_{218} := Vector_218
α_{219} := Vector_219
α_{220} := Vector_220
α_{221} := Vector_221
α_{222} := Vector_222
α_{223} := Vector_223
α_{224} := Vector_224
α_{225} := Vector_225
α_{226} := Vector_226
α_{227} := Vector_227
α_{228} := Vector_228
α_{229} := Vector_229
α_{230} := Vector_230
α_{231} := Vector_231
α_{232} := Vector_232
α_{233} := Vector_233
α_{234} := Vector_234
α_{235} := Vector_235
α_{236} := Vector_236
α_{237} := Vector_237
α_{238} := Vector_238
α_{239} := Vector_239
α_{240} := Vector_240
α_{241} := Vector_241
α_{242} := Vector_242
α_{243} := Vector_243
α_{244} := Vector_244
α_{245} := Vector_245
α_{246} := Vector_246
α_{247} := Vector_247
α_{248} := Vector_248
α_{249} := Vector_249
α_{250} := Vector_250

α_{50} := Vector_50
α_{51} := Vector_51
α_{52} := Vector_52
α_{53} := Vector_53
α_{54} := Vector_54
α_{55} := Vector_55
α_{56} := Vector_56
α_{57} := Vector_57
α_{58} := Vector_58
α_{59} := Vector_59
α_{60} := Vector_60
α_{61} := Vector_61
α_{62} := Vector_62
α_{63} := Vector_63
α_{64} := Vector_64
α_{65} := Vector_65
α_{66} := Vector_66
α_{67} := Vector_67
α_{68} := Vector_68
α_{69} := Vector_69
α_{70} := Vector_70
α_{71} := Vector_71
α_{72} := Vector_72
α_{73} := Vector_73
α_{74} := Vector_74
α_{75} := Vector_75
α_{76} := Vector_76
α_{77} := Vector_77
α_{78} := Vector_78
α_{79} := Vector_79
α_{80} := Vector_80
α_{81} := Vector_81
α_{82} := Vector_82
α_{83} := Vector_83
α_{84} := Vector_84
α_{85} := Vector_85
α_{86} := Vector_86
α_{87} := Vector_87
α_{88} := Vector_88
α_{89} := Vector_89
α_{90} := Vector_90
α_{151} := Vector_151
α_{152} := Vector_152
α_{153} := Vector_153
α_{154} := Vector_154
α_{155} := Vector_155
α_{156} := Vector_156
α_{157} := Vector_157
α_{158} := Vector_158
α_{159} := Vector_159
α_{160} := Vector_160
α_{161} := Vector_161
α_{162} := Vector_162
α_{163} := Vector_163
α_{164} := Vector_164
α_{165} := Vector_165
α_{166} := Vector_166
α_{167} := Vector_167
α_{168} := Vector_168
α_{169} := Vector_169
α_{170} := Vector_170
α_{171} := Vector_171
α_{172} := Vector_172
α_{173} := Vector_173
α_{174} := Vector_174
α_{175} := Vector_175
α_{176} := Vector_176
α_{177} := Vector_177
α_{178} := Vector_178
α_{179} := Vector_179
α_{180} := Vector_180
α_{181} := Vector_181
α_{182} := Vector_182
α_{183} := Vector_183
α_{184} := Vector_184
α_{185} := Vector_185
α_{186} := Vector_186
α_{187} := Vector_187
α_{188} := Vector_188
α_{189} := Vector_189
α_{190} := Vector_190
α_{191} := Vector_191
α_{251} := Vector_251
α_{252} := Vector_252
α_{253} := Vector_253
α_{254} := Vector_254
α_{255} := Vector_255
α_{256} := Vector_256
α_{257} := Vector_257
α_{258} := Vector_258
α_{259} := Vector_259
α_{260} := Vector_260
α_{261} := Vector_261
α_{262} := Vector_262
α_{263} := Vector_263
α_{264} := Vector_264
α_{265} := Vector_265
α_{266} := Vector_266
α_{267} := Vector_267
α_{268} := Vector_268
α_{269} := Vector_269
α_{270} := Vector_270
α_{271} := Vector_271
α_{272} := Vector_272
α_{273} := Vector_273
α_{274} := Vector_274
α_{275} := Vector_275
α_{276} := Vector_276
α_{277} := Vector_277
α_{278} := Vector_278
α_{279} := Vector_279
α_{280} := Vector_280
α_{281} := Vector_281
α_{282} := Vector_282
α_{283} := Vector_283
α_{284} := Vector_284
α_{285} := Vector_285
α_{286} := Vector_286
α_{287} := Vector_287
α_{288} := Vector_288
α_{289} := Vector_289
α_{290} := Vector_290
α_{291} := Vector_291

α_{91} := Vector_91
α_{92} := Vector_92
α_{93} := Vector_93
α_{94} := Vector_94
α_{95} := Vector_95
α_{96} := Vector_96
α_{97} := Vector_97
α_{98} := Vector_98
α_{99} := Vector_99
α_{100} := Vector_100

α_{192} := Vector_192
α_{193} := Vector_193
α_{194} := Vector_194
α_{195} := Vector_195
α_{196} := Vector_196
α_{197} := Vector_197
α_{198} := Vector_198
α_{199} := Vector_199
α_{200} := Vector_200

α_{292} := Vector_292
α_{293} := Vector_293
α_{294} := Vector_294
α_{295} := Vector_295
α_{296} := Vector_296
α_{297} := Vector_297
α_{298} := Vector_298
α_{299} := Vector_299
α_{300} := Vector_300

α_{301} := Vector_301
α_{302} := Vector_302
α_{303} := Vector_303
α_{304} := Vector_304
α_{305} := Vector_305
α_{306} := Vector_306
α_{307} := Vector_307
α_{308} := Vector_308
α_{309} := Vector_309
α_{310} := Vector_310
α_{311} := Vector_311
α_{312} := Vector_312
α_{313} := Vector_313
α_{314} := Vector_314
α_{315} := Vector_315
α_{316} := Vector_16
α_{317} := Vector_317
α_{318} := Vector_318
α_{319} := Vector_319
α_{320} := Vector_320
α_{321} := Vector_21
α_{322} := Vector_322
α_{323} := Vector_323
α_{324} := Vector_324
α_{325} := Vector_325
α_{326} := Vector_26
α_{327} := Vector_327
α_{328} := Vector_328
α_{329} := Vector_329
α_{330} := Vector_330

α_{331} := Vector_31
α_{332} := Vector_32
α_{333} := Vector_333
α_{334} := Vector_334
α_{335} := Vector_335
α_{336} := Vector_336
α_{337} := Vector_337
α_{338} := Vector_338
α_{339} := Vector_339
α_{340} := Vector_340
α_{341} := Vector_341
α_{342} := Vector_342
α_{343} := Vector_343
α_{344} := Vector_344
α_{345} := Vector_345
α_{346} := Vector_346
α_{347} := Vector_347
α_{348} := Vector_348
α_{349} := Vector_349
α_{350} := Vector_50
α_{351} := Vector_351
α_{352} := Vector_352
α_{353} := Vector_353
α_{354} := Vector_354
α_{355} := Vector_355
α_{356} := Vector_356
α_{357} := Vector_357
α_{358} := Vector_358
α_{359} := Vector_359

Frequencies Selections:

$f_{ref} := 1.7$

$$\lambda_{ref} := \frac{3 \cdot 10^8}{f_{ref} \cdot 10^9}$$

$\lambda_{ref} = 0.176$

$$d := \frac{\lambda_{ref}}{2}$$

$d = 0.088$

$freq_{oper} := 1.7$

$$\lambda := \frac{3 \cdot 10^8}{freq_{oper} \cdot 10^9}$$

$\lambda = 0.176$

$$k_{ref} := \frac{2 \cdot \pi}{\lambda_{ref}}$$

$k_{ref} = 35.605$

$$step_f := round\left(\frac{freq_{oper} - 0.8}{\Delta f}\right)$$

$step_f = 106$

$$k := \frac{2 \cdot \pi}{\lambda}$$

$k = 35.605$

Number of antenna elements:

$N := 30$

$n := 0 .. N - 1$

Transmitting direction:

$$\theta_{tx} := 10 \cdot \frac{\pi}{180}$$

$\theta_{tx} = 0.175$

Phase Reference

We will pick the furthest element as our reference element. The reference element has zero phase shift due to its location, because the position vector for this element is zero:

$$e^{j \cdot \frac{2 \cdot \pi}{\lambda} \cdot d \cdot n \cdot \sin(\theta_{tx})} = e^{j \cdot \frac{2 \cdot \pi}{\lambda} \cdot d \cdot 0 \cdot \sin(\theta_{tx})} = 1$$

Array Signals

Because of the array spatial distribution, there will be an additional phase shift assoicated with each element and each angle-of-transmission.

$$\Delta\psi := k_{ref} \cdot d \cdot \sin(\theta_{tx})$$

$$\Delta\psi := round\left(\Delta\psi \cdot \frac{180}{\pi}\right)$$

$\Delta\psi = 31$

There are 30 elements, thus there are 30 phasor values for the elements. Depending on the phase shift with respect to the reference element, the required phases for the elements are loaded into.

$x_0 := 0$

$x_1 := \text{if}(\Delta\psi < 0, \Delta\psi + 360, \text{mod}(\Delta\psi, 360))$

$x_2 := \text{mod}(x_1 + x_1, 360)$

$x_3 := \text{mod}(x_1 + x_2, 360)$

$x_4 := \text{mod}(x_1 + x_3, 360)$

$x_5 := \text{mod}(x_1 + x_4, 360)$

$x_6 := \text{mod}(x_1 + x_5, 360)$

$x_7 := \text{mod}(x_1 + x_6, 360)$

$x_8 := \text{mod}(x_1 + x_7, 360)$

$x_9 := \text{mod}(x_1 + x_8, 360)$

$x_9 := \text{mod}(x_1 + x_8, 360)$

$x_{10} := \text{mod}(x_1 + x_9, 360)$

$x_{11} := \text{mod}(x_1 + x_{10}, 360)$

$x_{12} := \text{mod}(x_1 + x_{11}, 360)$

$x_{13} := \text{mod}(x_1 + x_{12}, 360)$

$x_{14} := \text{mod}(x_1 + x_{13}, 360)$

$x_{15} := \text{mod}(x_1 + x_{14}, 360)$

$x_{16} := \text{mod}(x_1 + x_{15}, 360)$

$x_{17} := \text{mod}(x_1 + x_{16}, 360)$

$x_{18} := \text{mod}(x_1 + x_{17}, 360)$

$x_{19} := \text{mod}(x_1 + x_{18}, 360)$

$x_{20} := \text{mod}(x_1 + x_{19}, 360)$

$x_{21} := \text{mod}(x_1 + x_{20}, 360)$

$x_{22} := \text{mod}(x_1 + x_{21}, 360)$

$x_{23} := \text{mod}(x_1 + x_{22}, 360)$

$x_{24} := \text{mod}(x_1 + x_{23}, 360)$

$x_{25} := \text{mod}(x_1 + x_{24}, 360)$

$x_{26} := \text{mod}(x_1 + x_{25}, 360)$

$x_{27} := \text{mod}(x_1 + x_{26}, 360)$

$x_{28} := \text{mod}(x_1 + x_{27}, 360)$

$x_{29} := \text{mod}(x_1 + x_{28}, 360)$

$e^{j \cdot \Phi}$

component of the array factor

$\Phi el_0 := \left(\arg\left(\alpha_{x_0}\right)\right)_{step_f}$

$\Phi el_1 := \left(\arg\left(\alpha_{x_1}\right)\right)_{step_f}$

$\Phi el_2 := \left(\arg\left(\alpha_{x_2}\right)\right)_{step_f}$

$\Phi el_3 := \left(\arg\left(\alpha_{x_3}\right)\right)_{step_f}$

$\Phi el_4 := \left(\arg\left(\alpha_{x_4}\right)\right)_{step_f}$

$\Phi el_5 := \left(\arg\left(\alpha_{x_5}\right)\right)_{step_f}$

$\Phi el_6 := \left(\arg\left(\alpha_{x_6}\right)\right)_{step_f}$

$\Phi el_7 := \left(\arg\left(\alpha_{x_7}\right)\right)_{step_f}$

$\Phi el_8 := \left(\arg\left(\alpha_{x_8}\right)\right)_{step_f}$

$\Phi el_9 := \left(\arg\left(\alpha_{x_9}\right)\right)_{step_f}$

$\Phi el_{10} := \left(\arg\left(\alpha_{x_{10}}\right)\right)_{step_f}$

$\Phi el_{11} := \left(\arg\left(\alpha_{x_{11}}\right)\right)_{step_f}$

$\Phi el_{12} := \left(\arg\left(\alpha_{x_{12}}\right)\right)_{step_f}$

$\Phi el_{13} := \left(\arg\left(\alpha_{x_{13}}\right)\right)_{step_f}$

$\Phi el_{14} := \left(\arg\left(\alpha_{x_{14}}\right)\right)_{step_f}$

$\Phi el_{15} := \left(\arg\left(\alpha_{x_{15}}\right)\right)_{step_f}$

$\Phi el_{16} := \left(\arg\left(\alpha_{x_{16}}\right)\right)_{step_f}$

$\Phi el_{17} := \left(\arg\left(\alpha_{x_{17}}\right)\right)_{step_f}$

$\Phi el_{18} := \left(\arg\left(\alpha_{x_{18}}\right)\right)_{step_f}$

$\Phi el_{19} := \left(\arg\left(\alpha_{x_{19}}\right)\right)_{step_f}$

$\Phi el_{20} := \left(\arg\left(\alpha_{x_{20}}\right)\right)_{step_f}$

$\Phi el_{21} := \left(\arg\left(\alpha_{x_{21}}\right)\right)_{step_f}$

$\Phi el_{22} := \left(\arg\left(\alpha_{x_{22}}\right)\right)_{step_f}$

$\Phi el_{23} := \left(\arg\left(\alpha_{x_{23}}\right)\right)_{step_f}$

$\Phi el_{24} := \left(\arg\left(\alpha_{x_{24}}\right)\right)_{step_f}$

$\Phi el_{25} := \left(\arg\left(\alpha_{x_{25}}\right)\right)_{step_f}$

$\Phi el_{26} := \left(\arg\left(\alpha_{x_{26}}\right)\right)_{step_f}$

$\Phi el_{27} := \left(\arg\left(\alpha_{x_{27}}\right)\right)_{step_f}$

$\Phi el_{28} := \left(\arg\left(\alpha_{x_{28}}\right)\right)_{step_f}$

$\Phi el_{29} := \left(\arg\left(\alpha_{x_{29}}\right)\right)_{step_f}$

Amplitude read in based on the phase shift of the element with respect to the reference element.

$A_0 := \left|\left(\alpha_{x_0}\right)_{step_f}\right|$

$A_1 := \left|\left(\alpha_{x_1}\right)_{step_f}\right|$

$A_{10} := \left|\left(\alpha_{x_{10}}\right)_{step_f}\right|$

$A_{11} := \left|\left(\alpha_{x_{11}}\right)_{step_f}\right|$

$A_{20} := \left|\left(\alpha_{x_{20}}\right)_{step_f}\right|$

$A_{21} := \left|\left(\alpha_{x_{21}}\right)_{step_f}\right|$

$$A_2 := \left|\left(\alpha_{x_2}\right)_{step_f}\right| \quad A_{12} := \left|\left(\alpha_{x_{12}}\right)_{step_f}\right| \quad A_{22} := \left|\left(\alpha_{x_{22}}\right)_{step_f}\right|$$
$$A_3 := \left|\left(\alpha_{x_3}\right)_{step_f}\right| \quad A_{13} := \left|\left(\alpha_{x_{13}}\right)_{step_f}\right| \quad A_{23} := \left|\left(\alpha_{x_{23}}\right)_{step_f}\right|$$
$$A_4 := \left|\left(\alpha_{x_4}\right)_{step_f}\right| \quad A_{14} := \left|\left(\alpha_{x_{14}}\right)_{step_f}\right| \quad A_{24} := \left|\left(\alpha_{x_{24}}\right)_{step_f}\right|$$
$$A_5 := \left|\left(\alpha_{x_5}\right)_{step_f}\right| \quad A_{15} := \left|\left(\alpha_{x_{15}}\right)_{step_f}\right| \quad A_{25} := \left|\left(\alpha_{x_{25}}\right)_{step_f}\right|$$
$$A_6 := \left|\left(\alpha_{x_6}\right)_{step_f}\right| \quad A_{16} := \left|\left(\alpha_{x_{16}}\right)_{step_f}\right| \quad A_{26} := \left|\left(\alpha_{x_{26}}\right)_{step_f}\right|$$
$$A_7 := \left|\left(\alpha_{x_7}\right)_{step_f}\right| \quad A_{17} := \left|\left(\alpha_{x_{17}}\right)_{step_f}\right| \quad A_{27} := \left|\left(\alpha_{x_{27}}\right)_{step_f}\right|$$
$$A_8 := \left|\left(\alpha_{x_8}\right)_{step_f}\right| \quad A_{18} := \left|\left(\alpha_{x_{18}}\right)_{step_f}\right| \quad A_{28} := \left|\left(\alpha_{x_{28}}\right)_{step_f}\right|$$
$$A_9 := \left|\left(\alpha_{x_9}\right)_{step_f}\right| \quad A_{19} := \left|\left(\alpha_{x_{19}}\right)_{step_f}\right| \quad A_{29} := \left|\left(\alpha_{x_{29}}\right)_{step_f}\right|$$

$\Phi_{el}^{T} \cdot \frac{180}{\pi} =$

	0	1	2	3	4	5	6	7
0	-135.114	-102.36	-74.246	-46.277	-10.479	21.171	51.172	82.967

$A^{T} =$

	0	1	2	3	4	5	6	7	8	9
0	0.411	0.41	0.444	0.404	0.387	0.429	0.408	0.424	0.45	0.386

Array Factor:

$$AF(\theta) := \sum_{n=0}^{N-1} A_n \cdot e^{j \cdot \Phi_{el_n}} \cdot e^{-j \cdot k \cdot d \cdot n \cdot \sin(\theta)}$$

Plotting elevation radiation pattern:

Note that the referenced radiation pattern is plotted with operating frequency equals 1.7 GHz.

$N_{angles} := 180$

$n := 0 .. N_{angles} - 1$

$\Delta\theta := \frac{\pi}{N_{angles} - 1}$

$\Delta\theta = 0.018$

$\theta_{obs_n} := n \cdot \Delta\theta - \frac{\pi}{2}$

$mag\_array\_pattern_n := 20 \cdot \log\left(\left(\left|AF\left(\theta_{obs_n}\right)\right|\right)\right)$

$max\_val := max(mag\_array\_pattern)$

$max\_val = 21.755$

$max\_plot := ceil(max(max\_val))$

$max\_plot = 22$

$\theta_{tx\_round} := \Delta\theta \cdot round\left(\frac{\theta_{tx}}{\Delta\theta}\right)$

$\theta_{tx\_round} = 0.176$

$signal_n := if\left(\theta_{obs_n} = \theta_{tx\_round}, max\_plot, 0\right)$

$\theta_n := \left(if\left(mag\_array\_pattern_n = max\_val, \theta_{obs_n}, 0\right) \cdot \frac{180}{\pi} \right)$

$\theta_{max} := max(\theta)$

$\theta_{max} = 9.553$

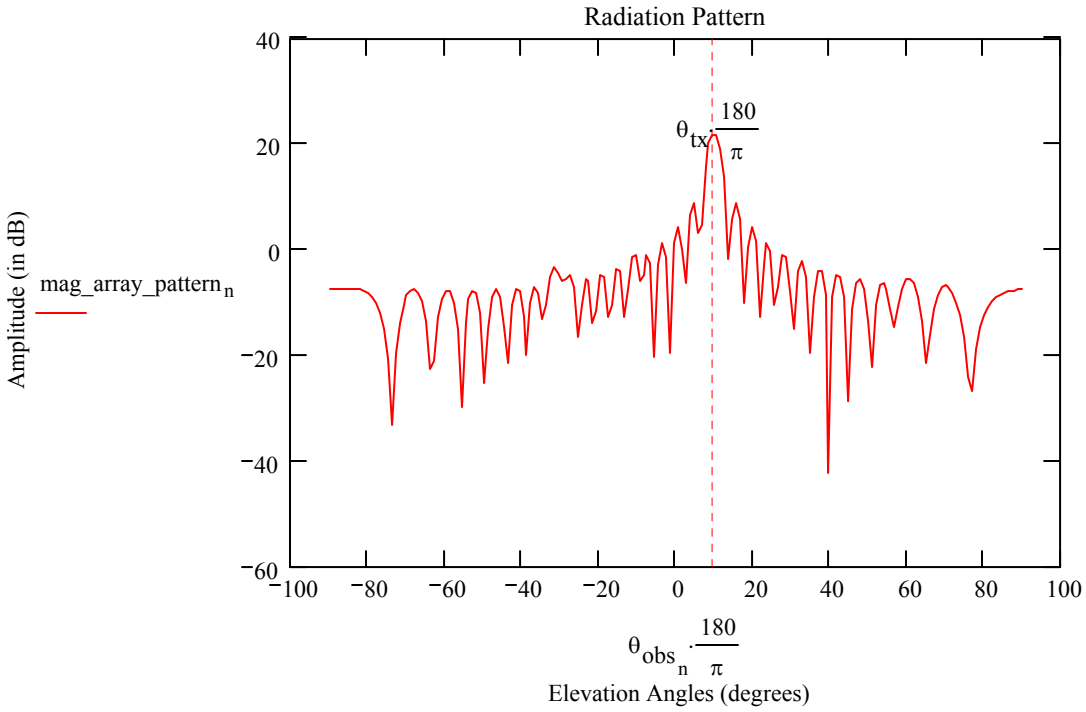

THIS PAGE INTENTIONALLY LEFT BLANK

APPENDIX D: MATLAB CODE FOR ARRAY RECEIVER

```
%This code is used to read in the measured I+, I-, Q+  and Q- from a data file “Demod_110102.m”.
% The single-ended I and Q components are converted to differential I and Q before computing the phases.

clear
load Demod_110103.m;
rad = pi/180;
degree = 180/pi;

phase_start = 0;
phase_stop = 355;
phase = [0:5:355];

%Read in IP, IN, QP & QN components.
IP = Demod_110103(:,1);
IN = Demod_110103(:,2);
QP = Demod_110103(:,3);
QN = Demod_110103(:,4);

%To get differential voltages.
Diff_I = (IP - IN);
Diff_Q = (QP - QN);

%Apply offset to the I & Q components.
Diff_I_off = Diff_I - 0.1;
Diff_Q_off = Diff_Q + 0.1;

%Measured phase, with and without offsets.
Phi = unwrap(atan2(Diff_Q,Diff_I))*(180/pi);
Phi_off = unwrap(atan2(Diff_Q_off,Diff_I_off));
Diff_I_max = max(Diff_I_off);
Diff_Q_max = max(Diff_Q_off);
A = Diff_I_max*cos(phase*rad);
B = Diff_Q_max*sin(phase*rad);

figure(1)
subplot(2,1,1)
plot(phase,Diff_I_off,phase,A,'x');
title('Transmitted Phase-In phase Response')
xlabel('Transmitted phase (degrees)'), ylabel('Measured differential In-Phase (volts)')
legend('Measured In-phase','Cosine')
subplot(2,1,2)
plot(phase,Diff_Q_off,phase,B,'x');
title('Transmitted Phase-Quadrature Response')
xlabel('Transmitted phase (degrees)'), ylabel('Measure differential Quadrature (volts)')
legend('Measured Quadrature','Sine')
print -depsc -tiff -r300 IQ

figure(2)
plot(phase,Phi)
title('Transmitted Phase-Measured Phase Response (w/o offsets)')
xlabel('Transmitted phase (degrees)'), ylabel('Measured phase (degrees)')
print -depsc -tiff -r300 phase_woff

%Theoretical result.
line = 1*phase + 100;
line0 = 1*phase + 0;

figure(3)
```

```
plot(phase,Phi_off*(180/pi),phase,line,'-')
title('Transmitted Phase-Measured Phase Resonse')
xlabel('Transmitted phase (degrees)'), ylabel('Measured phase (degrees)')
legend('Measured Phase','Theoretical Phase');
print -depsc -tiff -r300 phase_off

figure(4)
plot(phase,Phi_off*(180/pi)-100,phase,line0,'-')
title('Transmitted Phase-Measured Phase Resonse')
xlabel('Transmitted phase (degrees)'), ylabel('Measured phase (degrees)')
legend('Measured Phase','Theoretical Phase');
print -depsc -tiff -r300 phase_off_2

figure(5)
subplot(2,1,1)
plot(phase,Diff_I,phase,Diff_I_off);
title('In phase Component (without and with offset)')
xlabel('Transmitted phase (degrees)'), ylabel('Measured differential In-Phase (volts)')
legend('In-phase without offset','In-phase with offset')
subplot(2,1,2)
plot(phase,Diff_Q,phase,Diff_Q_off);
title('Quadrature Component (without and with offset)')
xlabel('Transmitted phase (degrees)'), ylabel('Measure differential Quadrature (volts)')
legend('Quadrature without offset','Quadrature with offset')
print -depsc -tiff -r300 IQ_2
```

LIST OF REFERENCES

[1] Jane's Navy International, http://www2.janes.com/janesdata/mags/jni/history/jni2003/images/p0548793.jpg, November 2003.

[2] Jane's Defense Weekly, http://www2.janes.com/janesdata/mags/jdw/history/jdw2003/images/p0530524.jpg, November 2003.

[3] L. C. Esswein, "Genetic algorithm design and testing of a random element 3-D 2.4 GHz phased array transmit antenna constructed of commercial RF microchips," Master's Thesis, Naval Postgraduate School, Monterey, California, June 2003.

[4] Jane's International Defense Review, http://www4.janes.com/K2/doc.jsp?t=A&K2DocKey=/content1/janesdata/mags/idr/history/idr96/idr00552.htm@current&QueryText=%3CAND%3E%28%3COR%3E%28naval+%3CAND%3E+radars+%3CAND%3E+IDR+%29%29&Prod_Name=IDR&, November 2003.

[5] C. A. Balanis, *Antenna Theory Analysis and Design*, 2nd edition, Wiley, New York, 1997.

[6] P.H. Lehne and M. Pettersen. "An overview of smart antenna technology for mobile communications systems," *IEEE Communications Surveys*, Vol. 2, No. 4, pp. 2-13, 1999.

[7] W.L. Stutzman and G. A. Thiele, *Antenna Theory and Design*, 2nd edition, pp. 405, Wiley, New York, 1998.

[8] D. P. Scolnik and J. O. Coleman, "Optimal design of wideband array patterns," *IEEE International Radar Conference*, pp. 172-177, 2000.

[9] C. Tarran, M Mitchell, and R. Howard, "Wideband phased array radar with digital adaptive beamforming," *High Resolution Radar and Sonar*, IEE Colloquium, pp. 1/1 – 1/7, 1999.

[10] D. J. Rabideau, "Improved wideband time delay beam-steering," *Thirty-fifth Asilomar Conference on Signals, Systems and Computers*, Vol. 2, pp. 1385-1390, 2001.

[11] J.Razavilar, F. Rashid-Farrokhi, and K. J. R. Liu, "Software radio architecture with smart antennas: a tutorial on algorithms and complexity," *IEEE Journal on Selected Areas in Communications*, Vol. 17, No. 4, pp. 662-676, 1999.

[12] D. L. Miroslav, J. L. Milan, and O. L. Borislav, "Analysis of SDMA & smart antenna techniques for existing and new mobile communication systems," http://www.telfor.org.yu/telfor2001/radovi/4-1.pdf, November 2003.

[13] J. Lebaric, Notes for EC4520 Wireless Propagation and Smart Antennas, Naval Postgraduate School, 2003 (unpublished).

[14] G. Ma, P. S. Hall, P. Gardner, and M. Hajian, "Direct downconversion active antennas for modulation and demodulation," *Proceedings of the 2nd International Conference on Microwave and Millimeter Wave Technology*, pp. 261-254, 2000.

[15] Analog Devices AD8346 Quadrature Modulator, http://www.analog.com/ UploadedFiles/Data_Sheets/646161894AD8346_0.pdf, November 2003.

[16] M. I. Skolnik, *Introduction to Radar Systems*, 3rd edition, pp. 566, McGraw Hill, New York, 2001.

[17] Analog Devices AD8347 Quadrature Demodulator, htttp://www.analog.com/UploadedFiles/Data_Sheets/756258393AD8347_0.pdf, November 2003.

[18] W. Namgoong and T. H. Meng, "Direct-conversion RF receiver design," *IEEE Trans. on Communications*, Vol. 49, No. 3, pp. 518-529, 2001.

INITIAL DISTRIBUTION LIST

1. Defense Technical Information Center
   Ft. Belvoir, Virginia

2. Dudley Knox Library
   Naval Postgraduate School
   Monterey, California

3. Professor John P. Powers
   Chairman, Department of Electrical and Computer Engineering
   Code EC
   Naval Postgraduate School
   Monterey, California

4. Professor Yeo Tat Soon
   Director, Temasek Defence Systems Institute
   Block E1, #05-05
   1, Engineering Drive 2
   Singapore 117576

5. Professor David C. Jenn
   Department of Electrical and Computer Engineering
   Code EC/Jn
   Naval Postgraduate School
   Monterey, California

6. Professor Roberto Cristi
   Department of Electrical and Computer Engineering
   Code EC/Cx
   Naval Postgraduate School
   Monterey, California

7. Professor Michael Melich
   Wayne E. Meyer Institute of System Engineering
   Naval Postgraduate School
   Monterey, California

8. Professor Rodney Johnson
   Wayne E. Meyer Institute of System Engineering
   Naval Postgraduate School
   Monterey, California

9. Cher Shin ENG
Ministry of Defense
Singapore